
Spherical Perspective on Learning with Batch Norm

Simon Roburin*

LIGM (UMR 8049), École des Ponts, UPE
valeo.ai

Yann de Mont-Marin*

Département d'informatique de l'ENS, PSL
Inria

Andrei Bursuc

valeo.ai

Renaud Marlet

valeo.ai

Patrick Pérez

valeo.ai

Mathieu Aubry

LIGM (UMR 8049), École des Ponts, UPE

Abstract

Batch Normalization (BN) is a prominent deep learning technique. In spite of its apparent simplicity, its implications over optimization are yet to be fully understood. In this paper, we study the optimization of neural networks with BN layers from a geometric perspective. We leverage the radial invariance of groups of parameters, such as neurons for multi-layer perceptrons or filters for convolutional neural networks, and translate several popular optimization schemes on the L_2 unit hypersphere. This formulation and the associated geometric interpretation sheds new light on the training dynamics and the relation between different optimization schemes. In particular, we use it to derive the effective learning rate of Adam and stochastic gradient descent (SGD) with momentum, and we show that in the presence of BN layers, performing SGD alone is actually equivalent to a variant of Adam constrained to the unit hypersphere. Our analysis also leads us to introduce new variants of Adam. We empirically show, over a variety of datasets and architectures, that they improve accuracy in classification tasks. The complete source code for our experiments is available at <https://github.com/ymontmarin/adamsrt>.

1 Introduction

The optimization process of deep neural networks is poorly understood. Their training involves minimizing a high-dimensional non-convex function, which has been proven to be a NP-hard problem [1]. Yet, elementary gradient-based methods show good results in practice. To improve the quality of reached minima, numerous methods have stemmed in the last years and have become common practices. One of the most prominent is Batch Normalization (BN) [2], which improves significantly both the stability of optimization and the performance of trained models, and is now used in most deep learning architectures. However, the interaction of BN with optimization and its link to regularization remain open research topics [3, 4, 5, 6].

One of the key effects of BN is to make neural networks (NN) invariant to positive scalings of groups of parameters. The core idea of this paper is precisely to focus on these groups of radially invariant parameters and analyze their optimization projected on the unit L_2 hypersphere (see Fig. 1), that is topologically equivalent to the quotient manifold of the parameter space by the scaling action. One could directly optimize parameters on the hypersphere [7]. Yet most optimization methods are still

*Equal contribution

performed successfully in the original parameter space. Instead, we propose to study and compare methods for a given group of radially invariant parameters through their image scheme on the unit hypersphere. It sheds new light on the interaction between normalization layers and optimization techniques. We believe this analysis is an important step towards a better understanding of the effect of BN on NN optimization, that would also include layer interaction. Please also note that, although our experiments here focus on BN, our approach could be applied to any radially invariant model.

The paper is organized as follows. In **Section 2**, we introduce our spherical framework to study the optimization of radially invariant models. We also define a generic notion of optimization scheme that encompasses methods such as SGD with momentum (SGD-M) and Adam [8]. We then derive its image step on the unit hypersphere, leading to definitions and expressions of *effective learning rate* and *effective learning direction*. In **Section 3**, we leverage the tools given by the spherical framework to study theoretically SGD. We show that SGD behaves like Adam without momentum, adapted and constrained to the hypersphere. In **Section 4**, we analyze the effective learning direction for Adam. The spherical framework highlights phenomena that cannot be easily translated into an optimization constrained to the hypersphere. We introduce the idea of *standardization* (S) and *rescale transport* of the momentum (RT) that neutralize these effects. Applied to Adam, it leads to new optimization schemes Adam-S and Adam-SRT. They empirically improve performance over a variety of architectures and classification datasets. In **Section 5**, these results are put in perspective with related work.

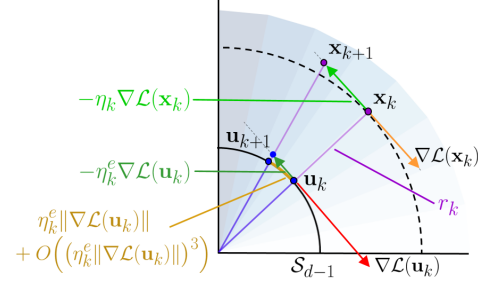


Figure 1: **Illustration of the spherical perspective for SGD.** The loss function \mathcal{L} of a NN w.r.t. the parameters $\mathbf{x}_k \in \mathbb{R}^d$ of a neuron followed by a BN is radially invariant. The neuron update $\mathbf{x}_k \rightarrow \mathbf{x}_{k+1}$ in the original space, with velocity $\eta_k \nabla \mathcal{L}(\mathbf{x}_k)$, corresponds to an update $\mathbf{u}_k \rightarrow \mathbf{u}_{k+1}$ of its projection through an exponential map on the unit hypersphere \mathcal{S}_{d-1} with velocity $\eta_k^e \|\nabla \mathcal{L}(\mathbf{u}_k)\|$ at order 2 (see details in Section 2.3).

Our main contributions are the following:

- A framework to analyze and compare optimization schemes of radially invariant models;
- A simple definition of the effective learning rate and its derivation for SGD-M and Adam, with and without L_2 regularization;
- The demonstration that, in the presence of BN layers, standard SGD behaves like Adam without momentum, constrained and adapted to the unit hypersphere;
- A new optimization scheme, Adam-SRT, showing significant accuracy boosts w.r.t. Adam.

2 Spherical framework for optimization

In this section, we provide background on radial invariance and introduce a generic optimization scheme. Projecting the scheme update on the unit hypersphere leads to the formal definitions of effective learning rate and learning direction. These expressions cast new light on the interaction between optimization and radially invariant parameters. The main notations are summarized in Fig. 1.

2.1 Radial invariance

We consider a family of parametric functions $\phi_{\mathbf{x}} : \mathbb{R}^{\text{in}} \rightarrow \mathbb{R}^{\text{out}}$ parameterized by a group of radially invariant parameters $\mathbf{x} \in \mathbb{R}^d \setminus \{\mathbf{0}\}$, i.e., $\forall \rho > 0, \phi_{\rho \mathbf{x}} = \phi_{\mathbf{x}}$ (possible other parameters of $\phi_{\mathbf{x}}$ are omitted for clarity), a dataset $\mathcal{D} \subset \mathbb{R}^{\text{in}} \times \mathbb{R}^{\text{out}}$, a loss function $\ell : \mathbb{R}^{\text{out}} \times \mathbb{R}^{\text{out}} \rightarrow \mathbb{R}$ and a training loss function $\mathcal{L} : \mathbb{R}^d \rightarrow \mathbb{R}$ defined as:

$$\mathcal{L}(\mathbf{x}) \stackrel{\text{def}}{=} \frac{1}{|\mathcal{D}|} \sum_{(\mathbf{s}, \mathbf{t}) \in \mathcal{D}} \ell(\phi_{\mathbf{x}}(\mathbf{s}), \mathbf{t}). \quad (1)$$

It verifies: $\forall \rho > 0, \mathcal{L}(\rho \mathbf{x}) = \mathcal{L}(\mathbf{x})$. In the context of NNs, the group of radially invariant parameters \mathbf{x} can be the parameters of a single neuron in a linear layer or the parameters of a whole filter in a

convolutional layer, followed by BN (see Appendix A for details, and Appendix B for the application to other normalization schemes such as InstanceNorm [9], LayerNorm [10] or GroupNorm [11]).

The quotient of the parameter space by the equivalence relation associated to radial invariance is topologically equivalent to a sphere. We consider here the L_2 sphere $\mathcal{S}_{d-1} = \{\mathbf{u} \in \mathbb{R}^d / \|\mathbf{u}\|_2 = 1\}$ as its canonical metric corresponds to angles: $d_S(\mathbf{u}_1, \mathbf{u}_2) = \arccos(\langle \mathbf{u}_1, \mathbf{u}_2 \rangle)$. This choice of metric is relevant to study NNs as filters in CNNs or neurons in MLPs, are applied through scalar product to input data. Besides, normalization in BN layers is also performed using the L_2 norm.

Our framework relies on the decomposition of vectors into radial and tangential components. During optimization, we write the radially invariant parameters at step $k \geq 0$ as $\mathbf{x}_k = r_k \mathbf{u}_k$ where $r_k = \|\mathbf{x}_k\|$ and $\mathbf{u}_k = \mathbf{x}_k / \|\mathbf{x}_k\|$. For any quantity $\mathbf{q}_k \in \mathbb{R}^d$ at step k , we write $\mathbf{q}_k^\perp = \mathbf{q}_k - \langle \mathbf{q}_k, \mathbf{u}_k \rangle \mathbf{u}_k$ its tangential component relative to the current direction \mathbf{u}_k .

The following lemma states that the gradient of a radially invariant loss function is tangential and -1 homogeneous:

Lemma 1 (Gradient of a function with radial invariance). *If $\mathcal{L} : \mathbb{R}^d \rightarrow \mathbb{R}$ is radially invariant and almost everywhere differentiable, then, for all $\rho > 0$ and all $\mathbf{x} \in \mathbb{R}^d$ where \mathcal{L} is differentiable:*

$$\langle \nabla \mathcal{L}(\mathbf{x}), \mathbf{x} \rangle = 0, \quad \nabla \mathcal{L}(\mathbf{x}) = \rho \nabla \mathcal{L}(\rho \mathbf{x}). \quad (2)$$

2.2 Generic optimization scheme

There is a large body of literature on optimization schemes [12, 13, 14, 8, 15]. We focus here on two of the most popular ones, namely SGD and Adam [8]. Yet, in order to establish general results that may apply to a variety of other schemes, we introduce here a *generic optimization update* as:

$$\mathbf{x}_{k+1} = \mathbf{x}_k - \eta_k \mathbf{a}_k \oslash \mathbf{b}_k, \quad (3)$$

$$\mathbf{a}_k = \beta \mathbf{a}_{k-1} + \nabla \mathcal{L}(\mathbf{x}_k) + \lambda \mathbf{x}_k, \quad (4)$$

where $\mathbf{x}_k \in \mathbb{R}^d$ is the group of radially invariant parameters at iteration k , \mathcal{L} is the group's loss estimated on a batch of input data, $\mathbf{a}_k \in \mathbb{R}^d$ is a momentum, $\mathbf{b}_k \in \mathbb{R}^d$ is a division vector that can depend on the trajectory $(\mathbf{x}_i, \nabla \mathcal{L}(\mathbf{x}_i))_{i \in \llbracket 0, k \rrbracket}$, $\eta_k \in \mathbb{R}$ is the scheduled trajectory-independent learning rate, \oslash denotes the Hadamard element-wise division, β is the momentum parameter, and λ is the L_2 regularization parameter. We show how it encompasses several known optimization schemes.

Stochastic gradient descent (SGD) has proven to be an effective optimization method in deep learning. It can include L_2 regularization (also called weight decay) and momentum. Its updates are:

$$\mathbf{x}_{k+1} = \mathbf{x}_k - \eta_k \mathbf{m}_k, \quad (5)$$

$$\mathbf{m}_k = \beta \mathbf{m}_{k-1} + \nabla \mathcal{L}(\mathbf{x}_k) + \lambda \mathbf{x}_k, \quad (6)$$

where \mathbf{m}_k is the momentum, β is the momentum parameter, and λ is the L_2 regularization parameter. It corresponds to our generic scheme Eq. (3-4) with $\mathbf{a}_k = \mathbf{m}_k$ and $\mathbf{b}_k = [1 \cdots 1]^\top$.

Adam [8] is likely the most common adaptive scheme for NNs. Its updates are:

$$\mathbf{x}_{k+1} = \mathbf{x}_k - \eta_k \frac{\mathbf{m}_k}{1 - \beta_1^{k+1}} \oslash \sqrt{\frac{\mathbf{v}_k}{1 - \beta_2^{k+1}}} + \epsilon, \quad (7)$$

$$\mathbf{m}_k = \beta_1 \mathbf{m}_{k-1} + (1 - \beta_1)(\nabla \mathcal{L}(\mathbf{x}_k) + \lambda \mathbf{x}_k), \quad \mathbf{v}_k = \beta_2 \mathbf{v}_{k-1} + (1 - \beta_2)(\nabla \mathcal{L}(\mathbf{x}_k) + \lambda \mathbf{x}_k)^2, \quad (8)$$

where \mathbf{m}_k is the momentum with parameter β_1 , \mathbf{v}_k is the order-2 moment with parameter β_2 , and ϵ prevents division by zero. (Here and in the following, the square and the square root of a vector are to be understood as element-wise). It corresponds to our generic scheme (Eqs. 3-4) with $\beta = \beta_1$ and:

$$\mathbf{a}_k = \frac{\mathbf{m}_k}{1 - \beta_1}, \quad \mathbf{b}_k = \frac{1 - \beta_1^{k+1}}{1 - \beta_1} \sqrt{\frac{\mathbf{v}_k}{1 - \beta_2^{k+1}}} + \epsilon. \quad (9)$$

2.3 Image optimization on the hypersphere

By analyzing our generic optimization update along its radial and tangential components, we obtain the following theorem which relates the update of radially invariant parameters in the parameter space \mathbb{R}^d and their update on \mathcal{S}_{d-1} through an exponential map.

Theorem 2 (Image step on \mathcal{S}_{d-1}). *The update of a group of radially invariant parameters \mathbf{x}_k at step k corresponds to an update of its projection \mathbf{u}_k on \mathcal{S}_{d-1} through an exponential map at \mathbf{u}_k with velocity $\eta_k^e \mathbf{c}_k^\perp$ at order 3:*

$$\mathbf{u}_{k+1} = \text{Exp}_{\mathbf{u}_k} \left(- \left[1 + O \left((\eta_k^e \|\mathbf{c}_k^\perp\|)^2 \right) \right] \eta_k^e \mathbf{c}_k^\perp \right), \quad (10)$$

where $\text{Exp}_{\mathbf{u}_k}$ is the exponential map on \mathcal{S}_{d-1} , and with

$$\mathbf{c}_k \stackrel{\text{def}}{=} r_k \mathbf{a}_k \oslash \frac{\mathbf{b}_k}{d^{-1/2} \|\mathbf{b}_k\|}, \quad \eta_k^e \stackrel{\text{def}}{=} \frac{\eta_k}{r_k^2 d^{-1/2} \|\mathbf{b}_k\|} \left(1 - \frac{\eta_k \langle \mathbf{c}_k, \mathbf{u}_k \rangle}{r_k^2 d^{-1/2} \|\mathbf{b}_k\|} \right)^{-1}. \quad (11)$$

More precisely:

$$\mathbf{u}_{k+1} = \frac{\mathbf{u}_k - \eta_k^e \mathbf{c}_k^\perp}{\sqrt{1 + (\eta_k^e \|\mathbf{c}_k^\perp\|)^2}}. \quad (12)$$

The proof is given in Appendix C.1.1 and the theorem is illustrated in the case of SGD in Fig. 1. Note that with typical values in CNN training we have $1 - \frac{\eta_k \langle \mathbf{c}_k, \mathbf{u}_k \rangle}{r_k^2 d^{-1/2} \|\mathbf{b}_k\|} > 0$ (cf. Appendix C.1.2).

Effective learning rate and direction. In Theorem 2, the normalized parameters update in Eq.10 can be read $\mathbf{u}_{k+1} \approx \text{Exp}_{\mathbf{u}_k} (-\eta_k^e \mathbf{c}_k^\perp)$ where η_k^e and \mathbf{c}_k^\perp can then be respectively interpreted as the learning rate and the direction of an optimization step constrained to \mathcal{S}_{d-1} . Because, \mathbf{a}_k is the momentum, and with Lemma 1, the quantity $r_k \mathbf{a}_k$ in \mathbf{c}_k is homogeneous to a momentum on the hypersphere. Due to the radial invariance, only the change of parameter on the unit hypersphere corresponds to a change of model function. Hence we can interpret η_k^e and \mathbf{c}_k^\perp as *effective learning rate* and *effective learning direction*. In other words, these quantities correspond to the learning rate and direction on the hypersphere that reproduce the function update of the optimization step.

Using the expression from Theorem 2, we can derive the effective learning rates for any optimization scheme that fits our generic framework, and in particular for SGD-M and Adam, with or without L_2 regularization (cf. Table 1). This is in contrast with learning rates in [3], that are approximate and asymptotic, and in [16], that are restricted to SGD only. To simplify and better analyze the formulas, as done for \mathbf{c}_k with \mathbf{a}_k , we introduce the quantity $\nu_k = r_k d^{-1/2} \|\mathbf{b}_k\|$, which is homogeneous to the norm of a gradient on the hypersphere, relating to an order-2 moment on the hypersphere.

Discussion. The division vector \mathbf{b}_k appears in two terms: a vector of deformation $\mathbf{b}_k / d^{-1/2} \|\mathbf{b}_k\|$ of norm $d^{1/2}$ equal to the norm of $[1 \cdots 1]^\top$ (the neutral element of Hadamard division), and a tuning of the learning rate by the scalar $d^{-1/2} \|\mathbf{b}_k\|$.

More interestingly, we can see that the learning rate is tuned by the dynamic of radiuses r_k :

$$\frac{r_{k+1}}{r_k} = \left(1 - \frac{\eta_k \langle \mathbf{c}_k, \mathbf{u}_k \rangle}{r_k^2 d^{-1/2} \|\mathbf{b}_k\|} \right) \sqrt{1 + (\eta_k^e \|\mathbf{c}_k^\perp\|)^2}. \quad (13)$$

Please note that, in contrast to [5], this result demonstrates that $\langle \mathbf{c}_k, \mathbf{u}_k \rangle$, which involves accumulated gradients terms in the momentum as well as L_2 regularization, also tunes the learning rate (cf. Fig.1). Note also that Weight Normalization (WN) [17], by keeping the radius constant during training, nullify this phenomenon of learning rate tuning.

Last, the amplitude of the step taken on the hypersphere reveals a dependence on the dimension d of the considered group of radially invariant parameters. In the case of an MLP or CNN that stacks layers with neurons or filters of different dimensions, the learning rate is thus tuned differently from one layer to another.

Table 1: Effective learning rate and direction for considered optimization schemes (iteration k omitted for clarity), where $\nu = r d^{-1/2} \|\mathbf{b}\|$. Adam-SRT, \mathbf{c}^{RT} and ν^{R} are defined in Sec. 4.2.

Scheme	η^e	\mathbf{c}^\perp
SGD	$\frac{\eta}{r^2}$	$\nabla \mathcal{L}(\mathbf{u})$
SGD + L_2	$\frac{\eta}{r^2(1-\eta\lambda)}$	$\nabla \mathcal{L}(\mathbf{u})$
SGD-M	$\frac{\eta}{r^2} \left(1 - \frac{\eta \langle \mathbf{c}, \mathbf{u} \rangle}{r^2} \right)^{-1}$	\mathbf{c}^\perp
Adam	$\frac{\eta}{r\nu} \left(1 - \frac{\eta \langle \mathbf{c}, \mathbf{u} \rangle}{r\nu} \right)^{-1}$	\mathbf{c}^\perp
Adam-SRT	$\frac{\eta}{r\nu^{\text{R}}} \left(1 - \frac{\eta\lambda r}{\nu^{\text{R}}} \right)^{-1}$	\mathbf{c}^{RT}

3 Application: analysis of SGD on the hypersphere

We leverage the tools introduced in the spherical framework to find a scheme constrained to the hypersphere equivalent to SGD. We show that for radially invariant models, SGD behaves like Adam without momentum, adapted and constrained to the unit hypersphere.

3.1 Equivalence between two optimization schemes

Due to the radial invariance, the functional space of the model is encoded by \mathcal{S}_{d-1} . In other words, two schemes with the same sequence of groups of radially invariant parameters on the hypersphere $(\mathbf{u}_k)_{k \geq 0}$, encode the same sequence of model functions. Two optimization schemes S and \tilde{S} are equivalent iff $\forall k \geq 0, \mathbf{u}_k = \tilde{\mathbf{u}}_k$. By using Eq.12, we obtain the following lemma, which is useful to prove the equivalence of two given optimization schemes:

Lemma 3 (Sufficient condition for the equivalence of optimization schemes).

$$\begin{cases} \mathbf{u}_0 = \tilde{\mathbf{u}}_0 \\ \forall k \geq 0, \eta_k^e = \tilde{\eta}_k^e, \mathbf{c}_k^\perp = \tilde{\mathbf{c}}_k^\perp \end{cases} \Rightarrow \forall k \geq 0, \mathbf{u}_k = \tilde{\mathbf{u}}_k. \quad (14)$$

3.2 A hypersphere-constrained scheme equivalent to SGD

We now study, within our spherical framework, SGD with L_2 regularization, i.e., the update $\mathbf{x}_{k+1} = \mathbf{x}_k - \eta_k(\nabla \mathcal{L}(\mathbf{x}_k) - \lambda_k \mathbf{x}_k)$. We know that SGD yields an adaptive behaviour because it is scheduled by the radius dynamic, which depends on gradients. Yet, the tools in our framework allow us to find a scheme constrained to the unit hypersphere equivalent to SGD. We relate SGD to a variant of AdamG [7], an adaptation of Adam constrained to the hypersphere. Dubbed AdamG*, it corresponds to the case of a null momentum factor $\beta_1 = 0$, a non-null initial order-2 moment v_0 , an offset of the scalar order-2 moment $k+1 \rightarrow k$ and the absence of the bias correction term $1 - \beta_2^{k+1}$:

$$\begin{aligned} \hat{\mathbf{x}}_{k+1} &= \mathbf{x}_k - \eta_k \frac{\nabla \mathcal{L}(\mathbf{x}_k)}{\sqrt{v_k}} \\ (\text{AdamG}^*) : \quad \mathbf{x}_{k+1} &= \frac{\hat{\mathbf{x}}_{k+1}}{\|\hat{\mathbf{x}}_{k+1}\|} \\ v_{k+1} &= \beta v_k + \|\nabla \mathcal{L}(\mathbf{x}_k)\|^2 \end{aligned}$$

Using Lemma 3, we can then show the following scheme equivalence (proof in Appendix C.1.3).

Theorem 4 (SGD equivalent scheme on the unit hypersphere). *For any $\lambda > 0, \eta > 0, r_0 > 0$, we have the following equivalence at order 2 in the radius dynamic:*

$$\begin{cases} (\text{SGD}) \\ \mathbf{x}_0 = r_0 \mathbf{u}_0 \\ \lambda_k = \lambda \\ \eta_k = \eta \end{cases} \text{ is scheme-equivalent at order 2 with } \begin{cases} (\text{AdamG}^*) \\ \mathbf{x}_0 = \mathbf{u}_0 \\ \beta = (1 - \eta\lambda)^4 \\ \eta_k = (2\beta)^{-1/2} \\ v_0 = r_0^4 (2\eta^2 \beta^{1/2})^{-1} \end{cases}$$

The notion of scheme equivalence offers a precise analysis of SGD for radially invariant parameters and highlights a link with Adam that was not expected at first. The scheduling performed by the radius dynamics actually replicates the effect of dividing the optimization step by the order-2 moment of the gradient norm.

4 Application: analysis of Adam on the hypersphere

In contrast to the direct theoretical analysis of SGD developed in Section 3.2, here we analyse Adam within the framework by highlighting phenomena that are not easily translated in the context of optimization constrained to the unit hypersphere. We propose two scheme transformations to neutralize these phenomena: standardization (S) and rescale transport (RT) of the momentum.

4.1 Standardization for Adam

Deformation. Considering the quantities defined for a generic scheme in Eq. 11, \mathbf{b}_k has a deformation effect $\frac{\mathbf{b}_k}{d^{-1/2} \|\mathbf{b}_k\|}$ on \mathbf{a}_k and a scheduling effect $d^{-1/2} \|\mathbf{b}_k\|$ on the effective learning rate. In the

case where the momentum factor $\beta_1 = 0$, the direction of the update at step k is $\nabla \mathcal{L}(\mathbf{u}_k) \oslash \frac{\mathbf{b}_k}{d^{-1/2}\|\mathbf{b}_k\|}$ (Eq. 11) and the deformation $\frac{\mathbf{b}_k}{d^{-1/2}\|\mathbf{b}_k\|}$ may push the direction of the update outside the tangent space of \mathcal{S}_{d-1} at \mathbf{u}_k (whereas the gradient itself lies in the tangent space). This deformation is in fact not isotropic: the displacement of the gradient from the tangent space depends on the position of \mathbf{u}_k on the sphere. We illustrate this anisotropy in Fig. 2(b).

Standardization (S). This anisotropy would not occur in the context of an optimization constrained to the hypersphere. In order to neutralize this anisotropic deformation while preserving the scheduling effect $d^{-1/2}\|\mathbf{b}_k\|$, we can adjust the scheme by normalizing \mathbf{b}_k , replacing it by $d^{1/2}\|\mathbf{b}_k\|[1 \cdots 1]^\top$ (see Appendix D.1). We call it *standardization* (S).

Adam-S. In the case of Adam, we show that the scheduling effect $d^{-1/2}\|\mathbf{b}_k\|$ corresponds to an order-2 moment of the gradient norm (see Appendix D.1). The standardization (S) consists in replacing the vector \mathbf{v}_k by the scalar v_k defined as:

$$v_k = \beta_2 v_{k-1} + (1 - \beta_2) d^{-1} \|\nabla \mathcal{L}(\mathbf{x}_k) + \lambda \mathbf{x}_k\|^2, \quad (15)$$

which is the 2nd-order moment of the gradient norm over the group of parameters. The new scheme is called *Adam-S*. Note that (the inverse of) the dimension d of the group of parameters naturally appears in this new order-2 moment. In the context of a CNN with a stack of layers of different filter dimensions, the learning rate differs for the different layers: the constant factor d^{-1} in the order-2 moment amounts to multiplying the learning rate η by $d^{1/2}$.

4.2 Rescaling and transport of the momentum for Adam

In the case of Adam with momentum, in order to analyse the impact of \mathbf{c}_k on the effective learning direction, we perform the following decomposition (cf. Appendix D.2):

$$\mathbf{c}_k = (\mathbf{c}_k^{\text{grad}} + \lambda r_k^2 \mathbf{c}_k^{L_2}) \oslash \frac{\mathbf{b}_k}{d^{-1/2}\|\mathbf{b}_k\|} \quad \text{with:} \quad (16)$$

$$\mathbf{c}_k^{\text{grad}} \stackrel{\text{def}}{=} \nabla \mathcal{L}(\mathbf{u}_k) + \sum_{i=0}^{k-1} \beta^{k-i} \frac{r_k}{r_i} \nabla \mathcal{L}(\mathbf{u}_i), \quad \mathbf{c}_k^{L_2} \stackrel{\text{def}}{=} \mathbf{u}_k + \sum_{i=0}^{k-1} \beta^{k-i} \frac{r_i}{r_k} \mathbf{u}_i. \quad (17)$$

The following quantities impact the effective learning direction with phenomena which would not occur in the case of a classical optimization constrained to the hypersphere:

1. The radius ratio $\frac{r_k}{r_i}$ present in both $\mathbf{c}_k^{\text{grad}}$ and $\mathbf{c}_k^{L_2}$ (in inverse proportion) impacts the effective learning direction \mathbf{c}_k^\perp : it can differ for identical sequences $(\mathbf{u}_i)_{i \leq k}$ on the sphere but with distinct radius histories $(r_i)_{i \leq k}$. Since the radius is closely related to the effective learning rate, it means the effective learning direction \mathbf{c}_k^\perp is adjusted according to the learning rates history.

2. Contribution of $\mathbf{c}_k^{\text{grad}}$. The contribution of each past gradient at step k corresponds to $\nabla \mathcal{L}(\mathbf{u}_i) - \langle \nabla \mathcal{L}(\mathbf{u}_i), \mathbf{u}_k \rangle \mathbf{u}_k$. It impacts the effective learning direction depending on its orientation relatively to \mathbf{u}_k . Two past points, although equally distant from \mathbf{u}_k on the sphere and with equal gradient amplitude may thus contribute very differently in \mathbf{c}_k^\perp due to their orientation (cf. Fig. 2(c)).

3. Contribution of $\mathbf{c}_k^{L_2}$. By definition, the current point \mathbf{u}_k does not contribute to the effective learning direction \mathbf{c}_k^\perp , unlike the history of points in $\sum_{i=0}^{k-1} \beta^{k-i} \frac{r_i}{r_k} \mathbf{u}_i$ that does. This dependency can be avoided if we decouple the L_2 regularization, because we do not accumulate L_2 terms in the momentum. This shows that the decoupling proposed in AdamW [15] actually removes the contribution of L_2 regularization in the effective learning direction.

The above effects, analyzed on the hypersphere, can be considered as undesirable. To cancel them, we adapt the momentum \mathbf{a}_k at each step.

Rescale and transport of the momentum (RT). To avoid the ratio $\frac{r_k}{r_i}$ in the effective learning direction and thus to cancel the *first effect*, we rescale the momentum in the update by the factor $\frac{r_{k-1}}{r_k}$ at each iteration $k \geq 1$. Furthermore, to avoid gradient history leaving the tangent space and thus neutralize the *second effect*, we perform a parallel transport (see Appendix D.2 for details) of the momentum \mathbf{a}_{k-1} from the corresponding point on the sphere \mathbf{u}_{k-1} to the new point \mathbf{u}_k at each iteration $k \geq 1$. The combination of rescaling and transport expressed as a rotation leads to the

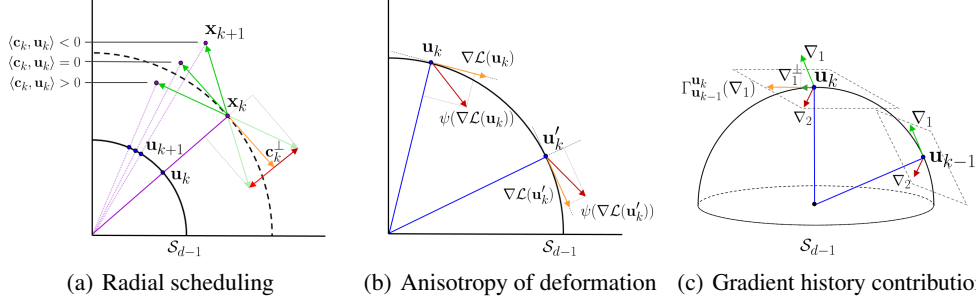


Figure 2: (a) Effect of the radial part of \mathbf{c}_k on the displacement on \mathcal{S}_{d-1} ; (b) Example of anisotropy and sign instability for the deformation $\psi(\nabla\mathcal{L}(\mathbf{u}_k)) = \nabla\mathcal{L}(\mathbf{u}_k) \oslash \frac{|\nabla\mathcal{L}(\mathbf{u}_k)|}{d^{-1/2}\|\nabla\mathcal{L}(\mathbf{u}_k)\|}$ (where $|\cdot|$ is the absolute value element-wise), typically occurring in Adam’s first optimization step; (c) Different contribution in \mathbf{c}_k^\perp of two past gradients ∇_1 and ∇_2 of equal norm, depending on their orientation. We also illustrate the transport of ∇_1 from \mathbf{u}_{k-1} to \mathbf{u}_k : $\Gamma_{\mathbf{u}_{k-1}}^{\mathbf{u}_k}(\nabla_1)$ (cf. Appendix D.2 for details)

formulation of the RT transformation (see Appendix D.2):

$$\text{RT}(\mathbf{a}_{k-1}) \stackrel{\text{def}}{=} \frac{\langle \mathbf{x}_k, \mathbf{x}_{k-1} \rangle \mathbf{a}_{k-1} - \langle \mathbf{x}_k, \mathbf{a}_{k-1} \rangle \mathbf{x}_{k-1}}{\langle \mathbf{x}_k, \mathbf{x}_k \rangle}. \quad (18)$$

Besides, we then have $\text{RT}(\mathbf{a}_{k-1} - \lambda \mathbf{u}_{k-1}) = \text{RT}(\mathbf{a}_{k-1})$, meaning that the L_2 contribution at step $k-1$ is not transported in the new momentum at step k . It is exactly a decoupling of the L_2 regularization which offsets the *third effect*.

Overall, the new momentum update reads $\mathbf{a}_k = \beta \text{RT}(\mathbf{a}_{k-1}) + \nabla\mathcal{L}(\mathbf{x}_k) + \lambda \mathbf{x}_k$ and leads to $\mathbf{c}_k = \mathbf{c}_k^{\text{RT}} + r_k^2 \lambda \mathbf{u}_k$ with a radial part $\langle \mathbf{c}_k, \mathbf{u}_k \rangle = \lambda r_k^2$ and an effective direction $\mathbf{c}_k^\perp = \mathbf{c}_k^{\text{RT}}$ that corresponds to the accumulated transported gradient on the hypersphere.

(RT) for Adam-S. Applying standardization (S) to Adam (cf. Section 4.1) keeps the gradients on the tangent space. We may then apply the RT transformation to Adam-S with momentum. We also rescale the order-2 moment v_k for consistency. Wrapping up, the new scheme Adam-SRT reads:

$$\mathbf{x}_{k+1} = \mathbf{x}_k - \eta_k \frac{\mathbf{m}_k}{1 - \beta_1^{k+1}} / \sqrt{\frac{v_k}{1 - \beta_2^{k+1}}} + \epsilon, \quad (19)$$

$$\mathbf{m}_k = \beta_1 \text{RT}(\mathbf{m}_{k-1}) + (1 - \beta_1)(\nabla\mathcal{L}(\mathbf{x}_k) + \lambda \mathbf{x}_k), \quad (20)$$

$$v_k = \beta_2 \frac{r_{k-1}^2}{r_k^2} v_{k-1} + (1 - \beta_2) d^{-1} \|\nabla\mathcal{L}(\mathbf{x}_k) + \lambda \mathbf{x}_k\|^2. \quad (21)$$

With these changes, Adam-SRT has a new scheduling effect denoted ν_k^{R} (cf. Appendix D.1) and an effective learning direction \mathbf{c}_k^{RT} (cf. Table 1), consistent with the hypersphere. The algorithm of Adam-SRT however only differs from Adam by a few lines of codes (cf. Algorithm 1 in Appendix E).

Remark. The RT transformation can also be applied to SGD-M. This variation, dubbed SGD-MRT, is studied in Appendix E.2, but we did not find it to lead to systematic performance improvements.

4.3 Empirical study of Adam and variation Adam-S, Adam-SRT

The previous section identified geometrical effects that are not easily translated into optimization on the hypersphere for Adam. The neutralization of these effects through standardisation (S) and rescale transport (RT) of the momentum lead to Adam-S and Adam-SRT. In the context of CNNs with BN, we evaluate our schemes over a variety of architectures and classification datasets.

Implementations of the new methods and the experimental protocol can be found here : <https://github.com/ymontmarin/adamsrt>.

CNNs with BN. The set of parameters θ of a CNN with BN layers can be split in two disjoint subsets: $\theta = \mathcal{F} \cup \mathcal{R}$, where \mathcal{F} is the set of groups of radially invariant parameters and \mathcal{R} the remaining parameters. As demonstrated in Appendix A, the subset \mathcal{F} includes parameters of all filters followed by BN. In the following, the proposed Adam variants are applied only to the optimization of the parameters in \mathcal{F} whereas the ones in \mathcal{R} are optimized with the original Adam scheme.

Table 2: Comparison of optimization scheme. The figures in this table are the mean top1 accuracy (and the standard deviation) over 5 seeds on the test set for CIFAR10, CIFAR100 and on the validation set for SVHN, and over 3 seeds for ImageNet. [†]In [15], improvements for AdamW were observed when using a cosine annealing scheduler; here we use fixed-frequency scheduling across all methods. [‡]In [7], SGD-M was used on the remaining group of parameters \mathcal{R} while here we used Adam for Adam-S, Adam-SRT and AdamG for comparison consistency.

Method	CIFAR10			CIFAR100		SVHN		ImageNet ResNet18
	ResNet20	ResNet18	VGG16	ResNet18	VGG16	ResNet18	VGG16	
SGD-M	92.39 (0.12)	95.10 (0.04)	93.56 (0.05)	77.08 (0.18)	73.77 (0.10)	95.96 (0.15)	95.95 (0.09)	69.86 (0.06)
Adam [8]	90.98 (0.06)	93.77 (0.20)	92.83 (0.17)	71.30 (0.36)	68.43 (0.16)	95.32 (0.23)	95.57 (0.20)	68.52 (0.10)
AdamW [15] [†]	90.19 (0.24)	93.61 (0.12)	92.53 (0.25)	67.39 (0.27)	71.37 (0.22)	95.38 (0.15)	95.60 (0.08)	-
AdamG [7] [‡]	91.64 (0.17)	94.67 (0.12)	93.41 (0.17)	73.76 (0.34)	70.17 (0.20)	95.73 (0.05)	95.70 (0.25)	-
Adam-S	91.15 (0.11)	93.95 (0.23)	92.92 (0.11)	74.44 (0.22)	68.73 (0.27)	95.75 (0.09)	95.66 (0.09)	68.82 (0.22)
Adam-SRT	<i>91.81</i> (0.20)	<i>94.92</i> (0.05)	93.75 (0.06)	75.28 (0.35)	<i>71.45</i> (0.13)	<i>95.84</i> (0.07)	<i>95.82</i> (0.05)	<i>68.93</i> (0.19)

Protocol. For evaluation we conduct experiments on two architectures, ResNet [18] in two flavors (ResNet20, a simple variant designed for small images [18], and ResNet18, a popular variant for image classification) and VGG16 [19] with BN, and on four datasets: SVHN [20], CIFAR10 [21], CIFAR100 and ImageNet [22]. We compare Adam-S and Adam-SRT against SGD-M, Adam [8], AdamW [15] and AdamG [7]. To ensure a fair evaluation, we perform extensive hyperparameter grid search for every combination of optimization method (for both proposed and baselines schemes), dataset and architecture, keeping the batch size fixed. All reported results are averaged over 5 different runs, except for ImageNet where we use 3 seeds. For all runs we use a fixed-frequency decay schedule of the learning rate with 3 jumps. We refer to Appendix E.1 for details of the grid-search, best hyperparameters found for each architecture and dataset. Since AdamG [7] does not need L_2 regularization on \mathcal{F} as the optimization is constrained to the hypersphere, we do not grid-search its L_2 regularization coefficient.

Results. We report results in Table 2. Overall, Adam-SRT consistently achieves better performance compared to Adam and its variants. We observe the most significant boosts on CIFAR100 for both ResNet and VGG, and on CIFAR10 for ResNet. The improvement holds for larger and more complex datasets such as ImageNet. Interestingly, our two transformations (S and RT) bridge the gap between Adam and SGD-M, almost matching it on CIFAR datasets. We find these results encouraging as Adam has been recently shown as the most practical scheme to reduce the computational cost of hyperparameter tuning, in particular for unknown datasets [23]. Adam-S improves accuracy over Adam, while Adam-SRT improves over Adam-S, hinting that the geometrical phenomena we studied play a significant role in the optimization process.

5 Related work

Understanding Batch Normalization. Albeit conceptually simple, BN has been shown to have complex implications over optimization. The argument of Internal Covariate Shift reduction [2] has been challenged and shown to be secondary to smoothing of optimization landscape [4, 24] or its modification by creating a different objective function [25], or enabling of high learning rates through improved conditioning [6]. Arora *et al.* [5] demonstrate that (S)GD with BN are robust to the choice of the learning rate, with guaranteed asymptotic convergence, while a similar finding for GD with BN is made in [26].

Invariances in neural networks. [7] propose optimizing over the Grassmann manifold using Riemannian GD. Liu *et al.* [27] project weights and activations on the unit hypersphere and compute a function of the angle between them instead of inner products, and subsequently generalize these operators by scaling the angle [28]. In [29] the radial invariance is leveraged to prove that weight decay (WD) can be replaced by an exponential learning rate scheduling for SGD with or without momentum. [5] investigates the radial invariance and show that radius dynamics depends on the past gradients, offering an adaptive behavior to the learning rate. Here we go further and show that SGD projected on the unit hypersphere corresponds to Adam constrained to the hypersphere, and we give an accurate definition of this adaptive behavior. WN [17] is an alternative solution to BN that normalizes weights instead of activations and leads to an adaptive regularization [30]. [31, 32] connect scale invariance from WN [17] with adaptive gradient methods [13] to design adaptive

schedules. WN keeps a neuron on a sphere of constant radius, while we analyze standard optimization schemes by looking at the equivalent step on a sphere and study their radius dynamic as a scheduling.

Effective learning rate. Due to its scale invariance, BN can adaptively adjust the learning rate [3, 7, 5, 29]. [3] shows that in BN-equipped networks, WD increases the effective learning rate by reducing the norm of the weights. Conversely, without WD, the norm grows unbounded [33], decreasing the effective learning rate. [34] brings additional evidence supporting hypothesis in [3], while [16] finds an exact formulation of the effective learning rate for SGD in normalized networks. In contrast with prior work, we find generic definitions of the effective learning rate with exact expressions for SGD and Adam.

6 Conclusion

The spherical framework introduced in this study provides a powerful tool to analyse optimization schemes through their projection on the L_2 unit hypersphere. It allows us to give a precise definition of the effective learning rate, to relate SGD to a form of Adam, and to propose improved variants of Adam after finely analyzing its behavior. The framework also brings light to existing optimization techniques such as weight decay decoupling or weight normalization. We believe that extensions of this approach to more complex invariances such as rescaling or permutation emerging when layers are stacked in NNs, could help towards a better understanding of optimization in deep learning.

Acknowledgements

All experiments in the paper were performed on the valeo.ai gpu cluster infrastructure. We thank Gabriel de Marmiesse for helping us with technical issues.

Broader Impact

Our work concerns theoretical aspects of optimization schemes, that can be used to improve them. An optimization scheme is a general device to select a “good” parameterization of a mathematical model in a sense to be fully defined by the mathematician using it (loss function to minimize), rather than imposed by our approach.

Consequently, our work does not have any direct ethical impact; it just can make an existing (or future) method perform better. Our wish is that it benefits to the research community as tool to improve knowledge on model behaviour and optimization.

For validating our approach, we experimented on image classification tasks. We only used publicly available academic datasets, and our work has not leveraged any possible bias in the data.

Issues regarding possible system failure and its consequences are not relevant in this context as we only propose variants of general optimization methods, although we did not prove formally that our variants retain the same safety properties as the original methods. The properties of these general optimization methods are anyway most often theoretically guaranteed only in simple cases and just empirically observed in broader settings.

Nevertheless, we can point out that a better optimization for the same training budget result in limiting the ecological impact of computation.

Finally, we strongly believe that a better theoretical understanding of deep learning, possibly using hints provided by experiments, is a crucial matter both scientifically and because of the impact of neural networks in the society. This understanding should help to structure research in the field while providing a better control on models, especially when they are used in critical applications.

References

- [1] Avrim Blum and Ronald L Rivest. Training a 3-node neural network is np-complete. In *Advances in neural information processing systems*, pages 494–501, 1989.

- [2] Sergey Ioffe and Christian Szegedy. Batch normalization: Accelerating deep network training by reducing internal covariate shift. In *32nd International Conference on Machine Learning (ICML)*, volume 37, pages 448–456, 2015.
- [3] Twan van Laarhoven. L2 regularization versus batch and weight normalization, 2017. arXiv preprint arXiv:1706.05350.
- [4] Shibani Santurkar, Dimitris Tsipras, Andrew Ilyas, and Aleksander Madry. How does batch normalization help optimization? In *Advances in Neural Information Processing Systems*, pages 2483–2493, 2018.
- [5] Sanjeev Arora, Zhiyuan Li, and Kaifeng Lyu. Theoretical analysis of auto rate-tuning by batch normalization. In *International Conference on Learning Representations (ICLR)*, 2019.
- [6] Nils Bjorck, Carla P Gomes, Bart Selman, and Kilian Q Weinberger. Understanding batch normalization. In *Advances in Neural Information Processing Systems*, pages 7694–7705, 2018.
- [7] Minhyung Cho and Jaehyung Lee. Riemannian approach to batch normalization. In *Advances in Neural Information Processing Systems*, pages 5225–5235, 2017.
- [8] Diederik P Kingma and Jimmy Ba. Adam: A method for stochastic optimization. In *International Conference on Learning Representations (ICLR)*, 2015.
- [9] Dmitry Ulyanov, Andrea Vedaldi, and Victor Lempitsky. Instance normalization: The missing ingredient for fast stylization. *arXiv preprint arXiv:1607.08022*, 2016.
- [10] Jimmy Lei Ba, Jamie Ryan Kiros, and Geoffrey E Hinton. Layer normalization. *arXiv preprint arXiv:1607.06450*, 2016.
- [11] Yuxin Wu and Kaiming He. Group normalization. In *Proceedings of the European Conference on Computer Vision (ECCV)*, pages 3–19, 2018.
- [12] Ilya Sutskever, James Martens, George Dahl, and Geoffrey Hinton. On the importance of initialization and momentum in deep learning. In Sanjoy Dasgupta and David McAllester, editors, *30th International Conference on Machine Learning (ICML)*, volume 28 of *Proceedings of Machine Learning Research*, pages 1139–1147, Atlanta, Georgia, USA, 17–19 Jun 2013. PMLR.
- [13] John Duchi, Elad Hazan, and Yoram Singer. Adaptive subgradient methods for online learning and stochastic optimization. *Journal of machine learning research*, 12(Jul):2121–2159, 2011.
- [14] Tijmen Tieleman and Geoffrey Hinton. Lecture 6.5-rmsprop: Divide the gradient by a running average of its recent magnitude. *COURSERA: Neural networks for machine learning*, 4(2):26–31, 2012.
- [15] Ilya Loshchilov and Frank Hutter. Decoupled weight decay regularization. In *International Conference on Learning Representations (ICLR)*, 2019.
- [16] Elad Hoffer, Ron Banner, Itay Golan, and Daniel Soudry. Norm matters: efficient and accurate normalization schemes in deep networks. In *Advances in Neural Information Processing Systems (NeurIPS)*, pages 2160–2170, 2018.
- [17] Tim Salimans and Durk P Kingma. Weight normalization: A simple reparameterization to accelerate training of deep neural networks. In *Advances in neural information processing systems (NeurIPS)*, pages 901–909, 2016.
- [18] Kaiming He, Xiangyu Zhang, Shaoqing Ren, and Jian Sun. Deep residual learning for image recognition. In *IEEE conference on computer vision and pattern recognition (CVPR)*, pages 770–778, 2016.
- [19] Karen Simonyan and Andrew Zisserman. Very deep convolutional networks for large-scale image recognition. In *International Conference on Learning Representations (ICLR)*, 2015.
- [20] Yuval Netzer, Tao Wang, Adam Coates, Alessandro Bissacco, Bo Wu, and Andrew Y Ng. Reading digits in natural images with unsupervised feature learning. In *NIPS Workshop on Deep Learning and Unsupervised Feature Learning*, 2011.
- [21] Alex Krizhevsky, Geoffrey Hinton, et al. Learning multiple layers of features from tiny images, 2009.
- [22] Olga Russakovsky, Jia Deng, Hao Su, Jonathan Krause, Sanjeev Satheesh, Sean Ma, Zhiheng Huang, Andrej Karpathy, Aditya Khosla, Michael Bernstein, et al. Imagenet large scale visual recognition challenge. *International Journal of Computer Vision (IJCV)*, 115(3):211–252, 2015.

- [23] Prabhu Teja Sivaprasad, Florian Mai, Thijs Vogels, Martin Jaggi, and François Fleuret. Optimizer benchmarking needs to account for hyperparameter tuning. *arXiv preprint arXiv:1910.11758*, 2019.
- [24] Behrooz Ghorbani, Shankar Krishnan, and Ying Xiao. An investigation into neural net optimization via hessian eigenvalue density. In *36th International Conference on Machine Learning (ICML)*, volume 97, pages 2232–2241. PMLR, 2019.
- [25] Xiangru Lian and Ji Liu. Revisit batch normalization: New understanding and refinement via composition optimization. In *The 22nd International Conference on Artificial Intelligence and Statistics*, pages 3254–3263, 2019.
- [26] Yongqiang Cai, Qianxiao Li, and Zuowei Shen. A quantitative analysis of the effect of batch normalization on gradient descent. In *36th International Conference on Machine Learning (ICML)*, volume 97. PMLR, 2019.
- [27] Weiyang Liu, Yan-Ming Zhang, Xingguo Li, Zhiding Yu, Bo Dai, Tuo Zhao, and Le Song. Deep hyperspherical learning. In *Advances in neural information processing systems (NeurIPS)*, pages 3950–3960, 2017.
- [28] Weiyang Liu, Zhen Liu, Zhiding Yu, Bo Dai, Rongmei Lin, Yisen Wang, James M Rehg, and Le Song. Decoupled networks. In *IEEE Conference on Computer Vision and Pattern Recognition (CVPR)*, pages 2771–2779, 2018.
- [29] Zhiyuan Li and Sanjeev Arora. An exponential learning rate schedule for deep learning. In *International Conference on Learning Representations (ICLR)*, 2020.
- [30] Xiaoxia Wu, Edgar Dobriban, Tongzheng Ren, Shanshan Wu, Zhiyuan Li, Suriya Gunasekar, Rachel Ward, and Qiang Liu. Implicit regularization of normalization methods. *arXiv preprint arXiv:1911.07956*, 2019.
- [31] Xiaoxia Wu, Rachel Ward, and Léon Bottou. WNGrad: Learn the learning rate in gradient descent. *arXiv preprint arXiv:1803.02865*, 2018.
- [32] Rachel Ward, Xiaoxia Wu, and Leon Bottou. AdaGrad stepsizes: Sharp convergence over nonconvex landscapes. In *International Conference on Machine Learning (ICML)*, pages 6677–6686, 2019.
- [33] Daniel Soudry, Elad Hoffer, Mor Shpigel Nacson, Suriya Gunasekar, and Nathan Srebro. The implicit bias of gradient descent on separable data. *The Journal of Machine Learning Research (JMLR)*, 19(1):2822–2878, 2018.
- [34] Guodong Zhang, Chaoqi Wang, Bowen Xu, and Roger Grosse. Three mechanisms of weight decay regularization. In *International Conference on Learning Representations (ICLR)*, 2019.

Supplementary Material to “Spherical Perspective on Learning with Batch Norm”

A Radial invariance of filters with BN

In this section, we show the radial invariance of a set of filters equipped with BN. Please note that the following notations are specific and restricted to this section.

For the sake of simplicity, we only consider the case of a convolutional layer that preserves the spatial extension of the input. We also focus on a single filter. Since all filters act independently on input data, the following calculation holds for any filter.

Let $\mathbf{x} \in \mathbb{R}^{C \times K}$ be the parameters of a single filter, where C is the number of input channels and K is the kernel size. During training, this layer is followed by BN and applied to a batch $\mathbf{s} \in \mathbb{R}^{B \times C \times D}$ of B inputs of spatial size D . The output of the convolution operator ϕ applied to a filter $\mathbf{x} \in \mathbb{R}^{C \times K}$ and to a given batch element $\mathbf{s}_b \in \mathbb{R}^{C \times D}$, with $b \in \llbracket 1, B \rrbracket$, is thus:

$$\mathbf{t}_b \stackrel{\text{def}}{=} \phi(\mathbf{x}, \mathbf{s}_b) \in \mathbb{R}^D. \quad (22)$$

The application $(\mathbf{x}, \mathbf{s}_b) \mapsto \phi(\mathbf{x}, \mathbf{s}_b)$ is bilinear. BN then centers and normalizes the output \mathbf{t} using the mean and variance over the batch and the spatial dimension:

$$\mu = \frac{1}{BD} \sum_{b,j} t_{b,j}, \quad (23)$$

$$\sigma^2 = \frac{1}{BD} \sum_{b,j} (t_{b,j} - \mu)^2, \quad (24)$$

$$\hat{\mathbf{t}}_b \stackrel{\text{def}}{=} (\sigma^2 + \epsilon)^{-1/2} (\mathbf{t}_b - \mu \mathbf{1}_D), \quad (25)$$

where $\mathbf{1}_D$ denotes the all-ones vector of dimension D and ϵ is a small constant.

Now if the coefficients of the filter are rescaled by $\rho > 0$, then, by bilinearity, the new output of the layer for this filter verifies:

$$\tilde{\mathbf{t}}_b = \phi(\rho \mathbf{x}, \mathbf{s}_b) = \rho \phi(\mathbf{x}, \mathbf{s}_b). \quad (26)$$

Since the variance of inputs is generally large in practice, for small ϵ , the mean and variance are:

$$\tilde{\mu} = \rho \mu, \quad (27)$$

$$\tilde{\sigma}^2 \approx \rho^2 \sigma^2. \quad (28)$$

It can then be considered that the subsequent BN layer is invariant to this rescaling, *i.e.*, $\hat{\tilde{\mathbf{t}}}_b \approx \hat{\mathbf{t}}_b$.

B Extension to other normalization layers

The radial invariance for BN described above in Appendix A applies as well to InstanceNorm (IN) [9] as the normalization is also done with respect to channels but without the batch dimension. Regarding LayerNorm [10] (LN), the normalization is performed over all channels and the entire weight layer can thus be rescaled too, without impacting the output. As for GroupNorm [11] (GN), it associates several channels for normalization; the radial invariance in this case concerns the corresponding group of filters.

Thanks to this general property of radial invariance, the results in this paper not only concern BN but also IN. In fact, they apply as well to LN and GN when considering the suitable group of parameters. The optimization in this case concerns the proper slice of the parameter tensor of the layer, *i.e.*, the whole tensor for LN, and the selected group of filters for GN.

C Results in Sections 2 and 3

In this section, we provide proofs and/or empirical results supporting the claims in Sections 2 and 3 of the paper.

In the following, the double parentheses around an equation number, e.g., ((10)), indicate that we recall an equation that was previously stated in the main paper, rather than introduce a new one, e.g., noted (29). Also, framed formulas actually refer to results stated in the main paper, thus with double-bracket equation numbering.

C.1 Proof of theorems and validity of assumptions

C.1.1 Proof of Theorem 2 (Image step on \mathcal{S}_{d-1}) in Section 2.3

We recall the main theorem in Section 2.3.

Theorem 2 (Image step on \mathcal{S}_{d-1}) *The update of a group of radially invariant parameters \mathbf{x}_k at step k corresponds to an update of its projection \mathbf{u}_k on \mathcal{S}_{d-1} through an exponential map at \mathbf{u}_k with velocity $\eta_k^e \mathbf{c}_k^\perp$:*

$$\mathbf{u}_{k+1} = \text{Exp}_{\mathbf{u}_k} \left(- \left[1 + O \left((\eta_k^e \|\mathbf{c}_k^\perp\|)^2 \right) \right] \eta_k^e \mathbf{c}_k^\perp \right), \quad ((10))$$

where $\text{Exp}_{\mathbf{u}_k}$ is the exponential map on \mathcal{S}_{d-1} , and with

$$\mathbf{c}_k \stackrel{\text{def}}{=} r_k \mathbf{a}_k \oslash \frac{\mathbf{b}_k}{d^{-1/2} \|\mathbf{b}_k\|}, \quad \eta_k^e \stackrel{\text{def}}{=} \frac{\eta_k}{r_k^2 d^{-1/2} \|\mathbf{b}_k\|} \left(1 - \frac{\eta_k \langle \mathbf{c}_k, \mathbf{u}_k \rangle}{r_k^2 d^{-1/2} \|\mathbf{b}_k\|} \right)^{-1}. \quad ((11))$$

More precisely:

$$\mathbf{u}_{k+1} = \frac{\mathbf{u}_k - \eta_k^e \mathbf{c}_k^\perp}{\sqrt{1 + (\eta_k^e \|\mathbf{c}_k^\perp\|)^2}}. \quad ((12))$$

Proof. To simplify the calculation in the demonstration, we introduce the following notation:

$$A_k \stackrel{\text{def}}{=} \frac{\eta_k}{r_k^2 d^{-1/2} \|\mathbf{b}_k\|}. \quad (29)$$

We first demonstrate the expression for the radius dynamics in Eq. (13) and the precise step for \mathbf{u} in Eq. (12). Then we use geometric arguments and a Taylor expansion to derive the update on the sphere stated in Eq.(10).

Radius dynamics. We first show Eq. (13), which we recall here using the A_k notation:

$$\frac{r_{k+1}}{r_k} = (1 - A_k \langle \mathbf{c}_k, \mathbf{u}_k \rangle) \sqrt{1 + (\eta_k^e \|\mathbf{c}_k^\perp\|)^2}. \quad ((13))$$

First, we rewrite the step of a generic scheme in Eqs. (3-4) along the radial and tangential directions and separate the division vector \mathbf{b}_k into its deformation $\frac{\mathbf{b}_k}{d^{-1/2} \|\mathbf{b}_k\|}$ and its scalar scheduling effect $d^{-1/2} \|\mathbf{b}_k\|$, as stated in the discussion:

$$\begin{aligned} r_{k+1} \mathbf{u}_{k+1} &= r_k \mathbf{u}_k - \frac{\eta_k}{d^{-1/2} \|\mathbf{b}_k\|} \mathbf{a}_k \oslash \frac{\mathbf{b}_k}{d^{-1/2} \|\mathbf{b}_k\|} \\ &= r_k \left[\mathbf{u}_k - \frac{\eta_k}{r_k^2 d^{-1/2} \|\mathbf{b}_k\|} r_k \mathbf{a}_k \oslash \frac{\mathbf{b}_k}{d^{-1/2} \|\mathbf{b}_k\|} \right] \\ &= r_k \left[\mathbf{u}_k - A_k r_k \mathbf{a}_k \oslash \frac{\mathbf{b}_k}{d^{-1/2} \|\mathbf{b}_k\|} \right]. \end{aligned} \quad (30)$$

We can note the appearance of a new term $r_k \mathbf{a}_k$. The vector \mathbf{a}_k is a gradient momentum and therefore homogeneous to a gradient. Using Lemma 1, $r_k \mathbf{a}_k$ is homogeneous to a gradient on the hypersphere and can be interpreted as the momentum on the hypersphere.

From Eq. (30), we introduce \mathbf{c}_k (the deformed momentum on hypersphere) as in Eq. (11) and decompose it into the radial and tangential components. We have:

$$\begin{aligned} \frac{r_{k+1}}{r_k} \mathbf{u}_{k+1} &= \mathbf{u}_k - A_k \mathbf{c}_k \\ &= (1 - A_k \langle \mathbf{c}_k, \mathbf{u}_k \rangle) \mathbf{u}_k - A_k \mathbf{c}_k^\perp. \end{aligned} \quad (31)$$

By taking the squared norm of the equation, we obtain:

$$\frac{r_{k+1}^2}{r_k^2} = (1 - A_k \langle \mathbf{c}_k, \mathbf{u}_k \rangle)^2 + (A_k \|\mathbf{c}_k^\perp\|)^2. \quad (32)$$

Making the assumption that $1 - A_k \langle \mathbf{c}_k, \mathbf{u}_k \rangle > 0$, which is true in practice and discussed in the next subsection, we have:

$$\frac{r_{k+1}}{r_k} = (1 - A_k \langle \mathbf{c}_k, \mathbf{u}_k \rangle) \sqrt{1 + \left(\frac{A_k}{1 - A_k \langle \mathbf{c}_k, \mathbf{u}_k \rangle} \|\mathbf{c}_k^\perp\| \right)^2}. \quad (33)$$

After introducing $\eta_k^e = \frac{A_k}{(1 - A_k \langle \mathbf{c}_k, \mathbf{u}_k \rangle)}$ as in Eq. (11), we obtain the result of (13).

Update of normalized parameters. We then show Eq. (12):

$$\boxed{\mathbf{u}_{k+1} = \frac{\mathbf{u}_k - \eta_k^e \mathbf{c}_k^\perp}{\sqrt{1 + (\eta_k^e \|\mathbf{c}_k^\perp\|)^2}}}. \quad ((12))$$

Combining the radius dynamics previously calculated with Eq. (31), we have:

$$\mathbf{u}_{k+1} = \frac{(1 - A_k \langle \mathbf{c}_k, \mathbf{u}_k \rangle) \mathbf{u}_k - A_k \mathbf{c}_k^\perp}{(1 - A_k \langle \mathbf{c}_k, \mathbf{u}_k \rangle) \sqrt{1 + \eta_k^e \|\mathbf{c}_k^\perp\|}} \quad (34)$$

$$= \frac{\mathbf{u}_k - \frac{A_k}{1 - A_k \langle \mathbf{c}_k, \mathbf{u}_k \rangle} \mathbf{c}_k^\perp}{\sqrt{1 + \eta_k^e \|\mathbf{c}_k^\perp\|}}. \quad (35)$$

Hence the result (12) using the definition of η_k^e .

This result provides a unique decomposition of the generic step as a step in $\text{span}(\mathbf{u}_k, \mathbf{c}_k^\perp)$ for the normalized filter (Eq. (12)) and as a radius update (Eq. (13)).

We split the rest of the proof of the theorem in three parts.

Distance covered on the sphere. The distance covered on the hypersphere \mathcal{S}_{d-1} by an optimization step is:

$$\text{dist}_{\mathcal{S}_{d-1}}(\mathbf{u}_{k+1}, \mathbf{u}_k) = \arccos(\langle \mathbf{u}_{k+1}, \mathbf{u}_k \rangle). \quad (36)$$

From Eq. (12) and with Lemma 1, we also have:

$$\langle \mathbf{u}_{k+1}, \mathbf{u}_k \rangle = \frac{1}{\sqrt{1 + (\eta_k^e \|\mathbf{c}_k^\perp\|)^2}}. \quad (37)$$

Therefore, $\text{dist}_{\mathcal{S}_{d-1}}(\mathbf{u}_{k+1}, \mathbf{u}_k) = \varphi(\eta_k^e \|\mathbf{c}_k^\perp\|)$ where $\varphi : z \mapsto \arccos\left(\frac{1}{\sqrt{1+z^2}}\right)$, which is equal to \arctan on \mathbb{R}_+ . Then a Taylor expansion at order 3 of \arctan yields for $\eta_k^e \|\mathbf{c}_k^\perp\|$:

$$\text{dist}_{\mathcal{S}_{d-1}}(\mathbf{u}_{k+1}, \mathbf{u}_k) = \eta_k^e \|\mathbf{c}_k^\perp\| + O\left((\eta_k^e \|\mathbf{c}_k^\perp\|)^3\right). \quad (38)$$

The Taylor expansion validity is discussed in the next subsection.

Exponential map on the sphere. Given a Riemannian manifold \mathcal{M} , for a point $\mathbf{u} \in \mathcal{M}$ there exists an open set \mathcal{O} of the tangent space $\mathcal{T}_{\mathbf{u}}\mathcal{M}$ containing $\mathbf{0}$, such that for any tangent vector $\mathbf{w} \in \mathcal{O}$ there is a unique geodesic (a path minimizing the local distance on \mathcal{M} when conserving the tangent velocity) $\gamma : [-1, 1] \rightarrow \mathcal{M}$ that is differentiable and such that $\gamma(0) = \mathbf{u}$ and $\gamma'(0) = \mathbf{w}$. Then, the exponential map of \mathbf{w} from \mathbf{u} is defined as $\text{Exp}_{\mathbf{u}}(\mathbf{w}) = \gamma(1)$.

In the case of the manifold \mathcal{S}_{d-1} , the geodesics are complete (they are well defined for any point $\mathbf{u} \in \mathcal{S}_{d-1}$ and any velocity $\mathbf{w} \in \mathcal{T}_{\mathbf{u}}\mathcal{S}_{d-1}$) and are the great circles: for any $\mathbf{u} \in \mathcal{S}_{d-1}$ and any $\mathbf{w} \in \mathcal{T}_{\mathbf{u}}\mathcal{S}_{d-1}$, the map $\psi : t \in \mathbb{R} \mapsto \text{Exp}_{\mathbf{u}}(t\mathbf{w})$ verifies $\psi(\mathbb{R}) = \mathcal{S}_{d-1} \cap \text{span}(\{\mathbf{u}, \mathbf{w}\})$ which is a great circle passing through \mathbf{u} with tangent \mathbf{w} . Furthermore, since the circumference of the great circle is 2π , we have that for any $\mathbf{p} \in \mathcal{S}_{d-1} \setminus \{-\mathbf{u}\}$ there is a unique \mathbf{w} verifying $\|\mathbf{w}\| < \pi$ such that $\mathbf{p} = \text{Exp}_{\mathbf{u}}(\mathbf{w})$ and we have:

$$\text{dist}_{\mathcal{S}_{d-1}}(\mathbf{u}, \mathbf{p}) = \|\mathbf{w}\| \text{ and } \langle \mathbf{p}, \mathbf{w} \rangle \geq 0. \quad (39)$$

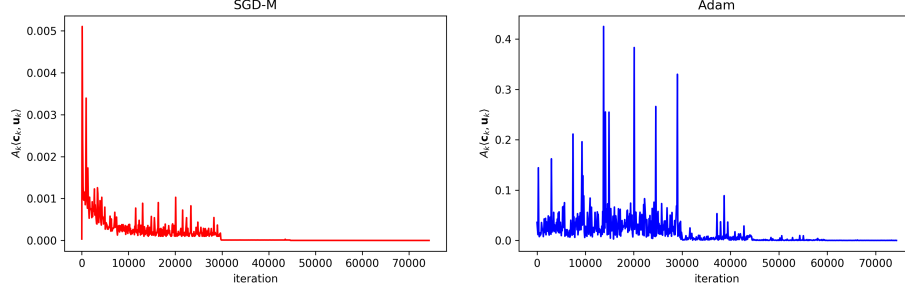


Figure 3: **Tracking of $A_k\langle \mathbf{c}_k, \mathbf{u}_k \rangle$ for SGD-M and Adam.** The above graphs show the maximum of the absolute value of $A_k\langle \mathbf{c}_k, \mathbf{u}_k \rangle$ for all filters in all layers of a ResNet20 CIFAR trained on CIFAR10 and optimized with SGD-M (left) or Adam (right). The quantity is always small compared to 1. Therefore we may assume that $1 - A_k\langle \mathbf{c}_k, \mathbf{u}_k \rangle \geq 0$.

Optimization step as an exponential map. We will use the previously stated differential geometry properties to prove:

$$\mathbf{u}_{k+1} = \text{Exp}_{\mathbf{u}_k} \left(- \left[1 + O \left((\eta_k^e \|\mathbf{c}_k^\perp\|)^2 \right) \right] \eta_k^e \mathbf{c}_k^\perp \right). \quad ((10))$$

For an optimization step we have:

- by construction, $\mathbf{c}_k^\perp \in \mathcal{T}_{\mathbf{u}_k} \mathcal{S}_{d-1}$;
- from Eq. (12), $\mathbf{u}_{k+1} \in \mathcal{S}_{d-1} \cap \text{span}(\{\mathbf{u}_k, \mathbf{c}_k^\perp\})$;
- from Eq. (12), $\langle \mathbf{u}_{k+1}, \mathbf{c}_k^\perp \rangle \leq 0$.

Then, there exists α that verifies $\|\alpha \mathbf{c}_k^\perp\| < \pi$ such that:

$$\mathbf{u}_{k+1} = \text{Exp}_{\mathbf{u}_k} (\alpha \mathbf{c}_k^\perp). \quad (40)$$

From Eq. (39), because $\langle \mathbf{u}_{k+1}, \mathbf{c}_k^\perp \rangle \leq 0$, we have $\alpha < 0$. We also have that $\|\alpha \mathbf{c}_k^\perp\| = \text{dist}_{\mathcal{S}_{d-1}}(\mathbf{u}_{k+1}, \mathbf{u}_k)$. Then, using the distance previously calculated in Eq. (38), we have:

$$|\alpha| \|\mathbf{c}_k^\perp\| = \eta_k^e \|\mathbf{c}_k^\perp\| + O \left((\eta_k^e \|\mathbf{c}_k^\perp\|)^3 \right), \quad (41)$$

$$|\alpha| = \eta_k^e \left[1 + O \left((\eta_k^e \|\mathbf{c}_k^\perp\|)^2 \right) \right]. \quad (42)$$

Combining the sign and absolute value of α , we get the final exponential map expression:

$$\mathbf{u}_{k+1} = \text{Exp}_{\mathbf{u}_k} \left(- \left[1 + O \left((\eta_k^e \|\mathbf{c}_k^\perp\|)^2 \right) \right] \eta_k^e \mathbf{c}_k^\perp \right), \quad ((10))$$

$$\approx \text{Exp}_{\mathbf{u}_k} (-\eta_k^e \mathbf{c}_k^\perp). \quad (43)$$

Note that we implicitly assume here that $|\alpha| \|\mathbf{c}_k^\perp\| \approx \eta_k^e \|\mathbf{c}_k^\perp\| < \pi$, which is discussed in the next subsection.

□

C.1.2 Validity of the assumptions in Theorem 2

Sign of $1 - A_k\langle \mathbf{c}_k, \mathbf{u}_k \rangle$. We tracked the maximum of the quantity $A_k\langle \mathbf{c}_k, \mathbf{u}_k \rangle$ for all the filters of a ResNet20 CIFAR trained on CIFAR10 and optimized with SGD-M or Adam (see Appendix E.3 for implementation details). As can be seen on Fig. 3, this quantity is always small compared to 1, making $1 - A_k\langle \mathbf{c}_k, \mathbf{u}_k \rangle$ always positive in practice. The order of magnitude of this quantity is roughly the same for different architectures and datasets.

Taylor expansion. We tracked the maximum of the quantity $\eta_k^e \|\mathbf{c}_k^\perp\|$ for all the filters of a ResNet20 CIFAR trained on CIFAR10 and optimized with SGD-M or Adam. The observed values justify the Taylor expansion and validate the assumption $|\alpha| \|\mathbf{c}_k^\perp\| \approx \eta_k^e \|\mathbf{c}_k^\perp\| < \pi$. (cf. Fig 4). The order of magnitude of this quantity is roughly the same for other different architectures and datasets.

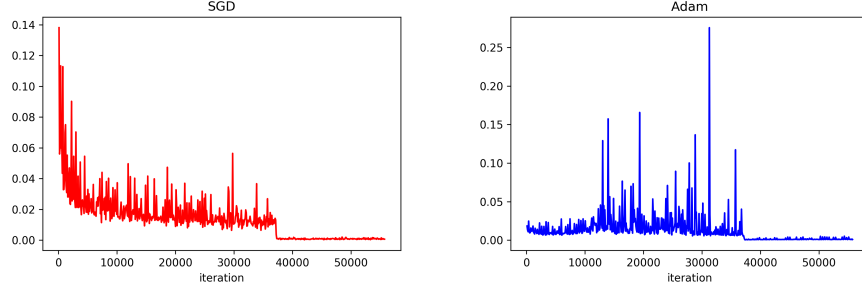


Figure 4: **Tracking of $\eta_k^e \|c_k^\perp\|$ for SGD-M and Adam.** The above graphs show the maximum of the absolute value of $\eta_k^e \|c_k^\perp\|$ for all filters in all layers of a ResNet20 CIFAR trained on CIFAR10 and optimized with SGD-M (left) or Adam (right).

C.1.3 Proof of Theorem 4 (SGD equivalent scheme on the unit hypersphere) in Section 3.2

We prove the following theorem:

Theorem 4 (SGD equivalent scheme on the unit hypersphere.) *For any $\lambda > 0, \eta > 0, r_0 > 0$, we have the following equivalence at order 2 in the radius dynamics:*

$$\left\{ \begin{array}{l} \text{(SGD)} \\ \mathbf{x}_0 = r_0 \mathbf{u}_0 \\ \lambda_k = \lambda \\ \eta_k = \eta \end{array} \right. \text{ is scheme-equivalent at order 2 to } \left\{ \begin{array}{l} \text{(AdamG*)} \\ \mathbf{x}_0 = \mathbf{u}_0 \\ \beta = (1 - \eta\lambda)^4 \\ \eta_k = (2\beta)^{-1/2} \\ v_0 = r_0^4 (2\eta^2 \beta^{1/2})^{-1} \end{array} \right.$$

Proof. As summarized in Table 1, the expressions of the effective learning rates and directions for SGD are $\mathbf{c}_k^\perp = r_k \nabla \mathcal{L}(\mathbf{x}_k) = \nabla \mathcal{L}(\mathbf{u}_k)$ and $\eta_k^e = \frac{\eta_k}{r_k^2(1 - \eta_k \lambda_k)}$.

Exponential scheduling effect of L_2 regularization. We look for conditions leading to an equivalence between SGD with L_2 regularization and SGD without L_2 regularization. Using Lemma 3, the equality of effective directions is trivial and the equality of effective learning rates for any step k yields the following equivalence:

$$\left\{ \begin{array}{l} \text{(SGD)} \\ \tilde{\mathbf{x}}_0 = r_0 \mathbf{u}_0 \\ \tilde{\lambda}_k = \lambda \\ \tilde{\eta}_k = \eta \end{array} \right. \text{ is scheme-equivalent to } \left\{ \begin{array}{l} \text{(SGD)} \\ \mathbf{x}_0 = r_0 \mathbf{u}_0 \\ \lambda_k = 0 \\ \eta_k = \eta(1 - \eta\lambda)^{-2k-1} \end{array} \right. \quad (44)$$

L_2 regularization is equivalent to an exponential scheduling of the learning rate, as found in [29]. To prove this statement in a constructive manner, we are going to use Lemma 3 and find a sufficient condition to have:

$$\left\{ \begin{array}{l} \text{(i) } \mathbf{u}_0 = \tilde{\mathbf{u}}_0 \\ \text{(ii) } \forall k \geq 0, \eta_k^e = \tilde{\eta}_k^e, \mathbf{c}_k^\perp = \tilde{\mathbf{c}}_k^\perp. \end{array} \right.$$

Equation (i) is trivially satisfied by simply taking the same starting point: $\tilde{\mathbf{x}}_0 = \mathbf{x}_0$.

Regarding (ii), because effective directions are the same and only depend on \mathbf{u}_k , we only need a sufficient condition on η_k^e . For effective learning rates, using Eq. (13) and expressions in Table 1, we have:

$$\eta_k^e = \tilde{\eta}_k^e \Leftrightarrow \frac{\eta_k}{r_k^2} = \frac{\tilde{\eta}_k}{\tilde{r}_k^2(1 - \tilde{\eta}_k \lambda)}. \quad (45)$$

Since $\tilde{\eta}_k = \eta$, we obtain:

$$(45) \Leftrightarrow \eta_k = \left(\frac{r_k}{\tilde{r}_k} \right)^2 \frac{\eta}{(1 - \eta\lambda)}.$$

Therefore:

$$\frac{\eta_{k+1}}{\eta_k} = \left(\frac{r_{k+1} \tilde{r}_k}{\tilde{r}_{k+1} r_k} \right)^2 = \left(\frac{r_{k+1}/r_k}{\tilde{r}_{k+1}/\tilde{r}_k} \right)^2.$$

By using the radius dynamics in Eq. (13) for the two schemes, SGD and SGD with L_2 regularization, and by the equality of effective learning rates and directions, we have:

$$\begin{aligned}\frac{\eta_{k+1}}{\eta_k} &= \left(\frac{\sqrt{1 + (\eta_k^e \|\mathbf{c}_k^\perp\|)^2}}{(1 - \eta\lambda)\sqrt{1 + (\tilde{\eta}_k^e \|\tilde{\mathbf{c}}_k^\perp\|)^2}} \right)^2 \\ &= (1 - \eta\lambda)^{-2}.\end{aligned}$$

By taking Eq. (45) for $k = 0$, because $r_0 = \tilde{r}_0$ we have: $\eta_0 = \eta(1 - \eta\lambda)^{-1}$. Combining the previous relation and the initialization case, we derive by induction that $\eta_k = \eta(1 - \eta\lambda)^{-2k-1}$ is a sufficient condition. We can conclude, using Lemma 3, the equivalence stated in Eq. (44).

Resolution of the radius dynamics. Without L_2 regularization, the absence of radial component in \mathbf{c}_k makes the radius dynamics simple:

$$r_{k+1}^2 = r_k^2 + \frac{(\eta_k \|\nabla \mathcal{L}(\mathbf{u}_k)\|)^2}{r_k^2}. \quad (46)$$

With a Taylor expansion at order 2, we can show that for $k \geq 1$ the solution $r_k^2 = \sqrt{2 \sum_{i=0}^{k-1} (\eta_i \|\nabla \mathcal{L}(\mathbf{u}_i)\|)^2 + r_0^4}$ satisfies the previous equation. Indeed using the expression at step $k + 1$ gives:

$$\begin{aligned}r_{k+1}^2 &= \sqrt{2 \sum_{i=0}^{k-1} (\eta_i \|\nabla \mathcal{L}(\mathbf{u}_i)\|)^2 + r_0^4 + 2(\eta_k \|\nabla \mathcal{L}(\mathbf{u}_k)\|)^2} \\ &= r_k^2 \sqrt{1 + 2 \frac{(\eta_k \|\nabla \mathcal{L}(\mathbf{u}_k)\|)^2}{r_k^4}} \\ &= r_k^2 \left(1 + (1/2) 2 \frac{(\eta_k \|\nabla \mathcal{L}(\mathbf{u}_k)\|)^2}{r_k^4} + o\left(\frac{(\eta_k \|\nabla \mathcal{L}(\mathbf{u}_k)\|)^2}{r_k^4}\right) \right) \\ &= r_k^2 + \frac{(\eta_k \|\nabla \mathcal{L}(\mathbf{u}_k)\|)^2}{r_k^2} + o\left(\frac{(\eta_k \|\nabla \mathcal{L}(\mathbf{u}_k)\|)^2}{r_k^2}\right).\end{aligned}$$

Using $\eta_k = \eta(1 - \eta\lambda)^{-2k-1}$, introducing $\beta = (1 - \eta\lambda)^4$, omitting the $o\left(\frac{(\eta_k \|\nabla \mathcal{L}(\mathbf{u}_k)\|)^2}{r_k^2}\right)$ and injecting the previous solution in the effective learning rate, we obtain the closed form:

$$\begin{aligned}\eta_k^e &= \frac{\eta(1 - \eta\lambda)^{-2k-1}}{\sqrt{2 \sum_{i=0}^{k-1} \eta^2 (1 - \eta\lambda)^{-4i-2} \|\nabla \mathcal{L}(\mathbf{u}_i)\|^2 + r_0^4}} \\ &= \frac{(2\beta)^{-\frac{1}{2}}}{\sqrt{\sum_{i=0}^{k-1} \beta^{(k-1)-i} \|\nabla \mathcal{L}(\mathbf{u}_i)\|^2 + \beta^k \frac{r_0^4}{2\eta^2 \beta^{\frac{1}{2}}}}}. \quad (47)\end{aligned}$$

AdamG*. The AdamG* scheme is constrained on the hypersphere thanks to the normalization; the radius is therefore constant and equal to 1. The absence of radial component in the update gives: $\mathbf{c}_k^\perp = \nabla \mathcal{L}(\mathbf{u}_k)$ and $\eta_k^e = \frac{\eta_k}{\sqrt{v_k}}$. Thus, the resolution of the induction on v_k leads to the closed form:

$$\eta_k^e = \frac{\eta_k}{\sqrt{\sum_{i=0}^{k-1} \beta^{(k-1)-i} \|\nabla \mathcal{L}(\mathbf{u}_i)\|^2 + \beta^k v_0}}. \quad (48)$$

Hence the final theorem, when identifying the closed-form expressions of effective learning rates and using Lemma 3. \square

C.1.4 Validity of the assumptions in Theorem 4

Validity of the Taylor expansion. We tracked, for a CNN trained with SGD, the quantity

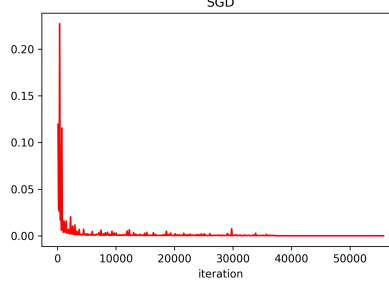


Figure 5: **Validity of Taylor expansion.** We tracked the maximum value of $(\eta_k \|\nabla \mathcal{L}(\mathbf{u}_k)\|)^2 / r_k^2$ for all filters in all layers of a ResNet20 CIFAR trained on CIFAR10 with SGD. The order of magnitude of the gradient is roughly the same for other architectures or datasets. It empirically validates the approximation by the Taylor expansion (see Appendix E.3 for implementation details).

$(\eta_k \|\nabla \mathcal{L}(\mathbf{u}_k)\|)^2 / r_k^2$, which is the variable of the Taylor expansion. As can be seen in Figure 5, the typical order of magnitude is 10^{-2} , justifying the Taylor expansion.

A quick formal analysis also suggests the validity of this hypothesis. Thanks to the expression of $\eta_k = (1 - \eta\lambda)^{-2i-k}\eta$ shown in the previous section, if we replace $\|\nabla \mathcal{L}(\mathbf{u}_k)\|$ by a constant for asymptotic analysis, the comparison becomes:

$$(1 - \eta\lambda)^{-4k-2} \ll (1 - \eta\lambda)^{-2} \frac{1 - (1 - \eta\lambda)^{-4k}}{1 - (1 - \eta\lambda)^{-4}} \quad (49)$$

$$1 \ll \frac{1 - (1 - \eta\lambda)^{4k}}{(1 - \eta\lambda)^{-4} - 1}. \quad (50)$$

It is asymptotically true.

D Results in Section 4 (Analysis of Adam on the hypersphere)

D.1 Results in Section 4.1 (Standardization for Adam)

Clarification on standardisation. Following Theorem 2, the division vector \mathbf{b}_k has two contributions in the decomposition:

- a deformation in \mathbf{c}_k applied to \mathbf{a}_k : $\mathbf{c}_k = r_k \mathbf{a}_k \oslash \frac{\mathbf{b}_k}{d^{-1/2} \|\mathbf{b}_k\|}$;
- a scheduling effect in the effective learning rate $d^{-1/2} \|\mathbf{b}_k\|$ (Eq. (11)).

The goal is to find a new division vector $\mathbf{S}(\mathbf{b}_k)$ that does not create a deformation while preserving the scheduling effect of \mathbf{b}_k in the effective learning rate. It means:

$$\frac{\mathbf{S}(\mathbf{b}_k)}{d^{-1/2} \|\mathbf{S}(\mathbf{b}_k)\|} = [1 \dots 1]^\top, \quad (51)$$

$$d^{-1/2} \|\mathbf{S}(\mathbf{b}_k)\| = d^{-1/2} \|\mathbf{b}_k\|. \quad (52)$$

This leads to $\mathbf{S}(\mathbf{b}_k) = d^{-1/2} \|\mathbf{b}_k\| [1 \dots 1]^\top$. Hence the substitution proposed in the paper.

In the case of $\beta_1 = 0$, $\mathbf{a}_k = \nabla \mathcal{L}(\mathbf{x}_k)$, for any \mathbf{b}_k . When we apply the standardisation, we obtain:

$$\mathbf{c}_k = r_k \nabla \mathcal{L}(\mathbf{x}_k) \oslash \frac{\mathbf{S}(\mathbf{b}_k)}{d^{-1/2} \|\mathbf{S}(\mathbf{b}_k)\|} = \nabla \mathcal{L}(\mathbf{u}_k) \oslash [1 \dots 1]^\top = \nabla \mathcal{L}(\mathbf{u}_k). \quad (53)$$

The direction lies in the tangent space because, by Lemma 1, the gradient belongs to it.

Details on Adam case. In the generic scheme, using the standardization gives:

$$\mathbf{x}_{k+1} = \mathbf{x}_k - \eta_k \mathbf{a}_k \oslash \mathbf{S}(\mathbf{b}_k) \quad (54)$$

$$= \mathbf{x}_k - \eta_k \mathbf{a}_k \oslash (d^{-1/2} \|\mathbf{b}_k\| [1 \dots 1]^\top) \quad (55)$$

$$= \mathbf{x}_k - \eta_k \mathbf{a}_k / (d^{-1/2} \|\mathbf{b}_k\|). \quad (56)$$

This means that the standardization consists in replacing the Hadamard division by \mathbf{b}_k with a scalar division by $d^{-1/2} \|\mathbf{b}_k\|$.

In the case of Adam, we recall that:

$$\mathbf{b}_k = \frac{1 - \beta_1^{k+1}}{1 - \beta_1} \sqrt{\frac{\mathbf{v}_k}{1 - \beta_2^{k+1}}} + \epsilon. \quad ((9))$$

Omitting ϵ for simplicity we have:

$$d^{-1/2} \|\mathbf{b}_k\| = \frac{1 - \beta_1^{k+1}}{1 - \beta_1} \left(\frac{1}{1 - \beta_2^{k+1}} \right)^{\frac{1}{2}} d^{-1/2} \|\sqrt{\mathbf{v}_k}\|. \quad (57)$$

Let us calculate $\|\sqrt{\mathbf{v}_k}\|$. Developing the recursion of \mathbf{v}_k , as defined in Eq. (8), leads to:

$$\mathbf{v}_k = (1 - \beta_2) \sum_{i=0}^k \beta_2^{k-i} (\nabla \mathcal{L}(\mathbf{x}_i) + \lambda \mathbf{x}_i)^2, \quad (58)$$

$$\sqrt{\mathbf{v}_k} = \sqrt{1 - \beta_2} \sqrt{\sum_{i=0}^k \beta_2^{k-i} (\nabla \mathcal{L}(\mathbf{x}_i) + \lambda \mathbf{x}_i)^2}, \quad (59)$$

where the square and the square-root are element-wise operations. Hence, if we take the square norm:

$$\begin{aligned} \|\sqrt{\mathbf{v}_k}\|^2 &= (1 - \beta_2) \sum_{j=1}^d \left(\sqrt{\sum_{i=0}^k \beta_2^{k-i} (\nabla \mathcal{L}(\mathbf{x}_i) + \lambda \mathbf{x}_i)^2} \right)_j^2 \\ &= (1 - \beta_2) \sum_{j=1}^d \sum_{i=0}^k \beta_2^{k-i} (\nabla \mathcal{L}(\mathbf{x}_i) + \lambda \mathbf{x}_i)_j^2 \\ &= (1 - \beta_2) \sum_{i=0}^k \beta_2^{k-i} \sum_{j=1}^d (\nabla \mathcal{L}(\mathbf{x}_i) + \lambda \mathbf{x}_i)_j^2 \\ &= (1 - \beta_2) \sum_{i=0}^k \beta_2^{k-i} \|\nabla \mathcal{L}(\mathbf{x}_i) + \lambda \mathbf{x}_i\|^2, \end{aligned} \quad (60)$$

where the j subscript denotes the j -th element of the vector. It is exactly the order-2 moment of the gradient norm.

Therefore, we define the scalar v_k :

$$v_k = \beta_2 v_{k-1} + (1 - \beta_2) d^{-1} \|\nabla \mathcal{L}(\mathbf{x}_k) + \lambda \mathbf{x}_k\|^2, \quad ((15))$$

which is the order-2 moment of the gradient norm with a factor d^{-1} . It verifies $\sqrt{v_k} = d^{-1/2} \|\sqrt{\mathbf{v}_k}\|$, needed for the scalar division stated in Eq. (57). By applying the bias correction, it gives the standardisation version of Adam, i.e., Adam-S:

$$\mathbf{x}_{k+1} = \mathbf{x}_k - \eta_k \frac{\mathbf{m}_k}{1 - \beta_1^{k+1}} / \sqrt{\frac{v_k}{1 - \beta_2^{k+1}}} + \epsilon, \quad (61)$$

$$\mathbf{m}_k = \beta_1 \mathbf{m}_{k-1} + (1 - \beta_1) (\nabla \mathcal{L}(\mathbf{x}_k) + \lambda \mathbf{x}_k), \quad (62)$$

$$v_k = \beta_2 v_{k-1} + (1 - \beta_2) d^{-1} \|\nabla \mathcal{L}(\mathbf{x}_k) + \lambda \mathbf{x}_k\|^2. \quad (63)$$

Note that the previous demonstration makes the factor d^{-1} appear in v_k to have exactly the scheduling effect of Adam without the deformation.

Scheduling effect of Adam division vector. With Eq. (60) and using Lemma 1, we can give the expression of the second-order moment on the sphere, defined as $\nu_k = r_k d^{-1/2} \|\mathbf{b}_k\|$:

$$\nu_k = d^{-1/2} \frac{1 - \beta_1^{k+1}}{1 - \beta_1} \left(\frac{1 - \beta_2}{1 - \beta_2^{k+1}} \right)^{1/2} \left(\sum_{i=0}^k \beta_2^{k-i} \frac{r_k^2}{r_i^2} \|\nabla \mathcal{L}(\mathbf{u}_i) + \lambda r_i^2 \mathbf{u}_i\|^2 \right)^{1/2}. \quad (64)$$

D.2 Results in Section 4.2 (Rescaling and transport of the momentum for Adam)

Decomposition of the effective direction. We decompose the effective direction as a gradient term and an L_2 regularization term:

$$\mathbf{c}_k^{\text{grad}} = \nabla \mathcal{L}(\mathbf{u}_k) + \sum_{i=0}^{k-1} \beta^{k-i} \frac{r_k}{r_i} \nabla \mathcal{L}(\mathbf{u}_i), \quad ((17))$$

$$\mathbf{c}_k^{L_2} = \mathbf{u}_k + \sum_{i=0}^{k-1} \beta^{k-i} \frac{r_i}{r_k} \mathbf{u}_i. \quad ((17))$$

Note that these expressions highlight the main terms at step k and the dependency on r_i .

Developing the recurrence in Eq (4), we obtain:

$$\mathbf{a}_k = \sum_{i=0}^k \beta^{k-i} (\nabla \mathcal{L}(\mathbf{x}_i) + \lambda \mathbf{x}_i). \quad (65)$$

Using Lemma 1 and decomposing on $\nabla \mathcal{L}(\mathbf{u}_i)$ and \mathbf{u}_i , we have:

$$\mathbf{a}_k = \sum_{i=0}^k \beta^{k-i} \left(\frac{1}{r_i} \nabla \mathcal{L}(\mathbf{u}_i) + \lambda r_i \mathbf{u}_i \right) \quad (66)$$

$$= \frac{1}{r_k} \left(\sum_{i=0}^k \beta^{k-i} \left(\frac{r_k}{r_i} \nabla \mathcal{L}(\mathbf{u}_i) + \lambda r_k r_i \mathbf{u}_i \right) \right). \quad (67)$$

Thus:

$$r_k \mathbf{a}_k = \sum_{i=0}^k \beta^{k-i} \frac{r_k}{r_i} \nabla \mathcal{L}(\mathbf{u}_i) + \lambda r_k^2 \sum_{i=0}^k \beta^{k-i} \frac{r_i}{r_k} \mathbf{u}_i, \quad (68)$$

which leads to the expression of $\mathbf{c}_k^{\text{grad}}$ and $\mathbf{c}_k^{L_2}$ when we define $\mathbf{c}_k \stackrel{\text{def}}{=} r_k \mathbf{a}_k \oslash \frac{\mathbf{b}_k}{d^{-1/2} \|\mathbf{b}_k\|}$ (Eq. (11)).

Precision on the RT transformation.

We introduce the rescaling and transport transformation of the momentum to neutralize the identified effects on the effective direction (cf. Section 4.2). The resulting, new \mathbf{c}_k is orthogonal to \mathbf{u}_k and does not contribute in the effective learning rate tuning with its radial part.

First, we rescale the momentum (\mathbf{a}_k in Eq. (3)) by a factor $\frac{r_{k-1}}{r_k}$ at iteration $k \geq 1$. From Lemma. 1, we obtain:

$$\mathbf{R}(\mathbf{a}_{k-1}) \stackrel{\text{def}}{=} \frac{r_{k-1}}{r_k} \mathbf{a}_{k-1} \quad (69)$$

$$\mathbf{a}_k = \beta \mathbf{R}(\mathbf{a}_{k-1}) + \nabla \mathcal{L}(\mathbf{x}_k) + \lambda \mathbf{x}_k \quad (70)$$

$$= \frac{1}{r_k} \left(\sum_{i=0}^k \beta^{k-i} (\nabla \mathcal{L}(\mathbf{u}_i) + \lambda r_i \mathbf{u}_i) \right). \quad (71)$$

Note that now, the factor $\frac{r_k}{r_i}$ is not contained anymore in the gradient contribution of $\mathbf{c}_k = r_k \mathbf{a}_k$, which neutralizes the first effect.

We then perform a parallel transport of the momentum \mathbf{a}_k from the corresponding point on the sphere \mathbf{u}_{k-1} to the new point \mathbf{u}_k , denoted as $\Gamma_{\mathbf{u}_{k-1}}^{\mathbf{u}_k}(\mathbf{a}_{k-1})$. Figure 2(c) illustrates the transport of a gradient. The parallel transport between two points associates each vector of the tangent space of the first point to a vector of the second tangent space by preserving the scalar product with the derivatives along the geodesic. Consequently, the gradients accumulated in the resulting momentum now lie in the tangent space of \mathbf{u}_k at each step. This neutralizes the second effect. Since \mathbf{u}_{k-1} , \mathbf{u}_k and \mathbf{a}_k are coplanar, the transport of the momentum on the hypersphere can be expressed as a rotation:

$$\mathbf{T}(\mathbf{a}_{k-1}) \stackrel{\text{def}}{=} \Gamma_{\mathbf{u}_{k-1}}^{\mathbf{u}_k}(\mathbf{a}_{k-1}) = \langle \mathbf{u}_{k-1}, \mathbf{u}_k \rangle \mathbf{a}_{k-1} - \langle \mathbf{a}_{k-1}, \mathbf{u}_k \rangle \mathbf{u}_{k-1}, \quad (72)$$

$$\mathbf{a}_k = \beta \mathbf{T}(\mathbf{a}_{k-1}) + \nabla \mathcal{L}(\mathbf{x}_k) + \lambda \mathbf{x}_k. \quad (73)$$

Although the transport operation is strictly defined on the tangent space only, the scalar product formulation enables its extension to the whole space. The transformation is linear and $\mathbf{T}(\mathbf{u}_{k-1}) = 0$. We thus have:

$$\mathbf{T}(\mathbf{a}_{k-1} - \lambda \mathbf{u}_{k-1}) = \mathbf{T}(\mathbf{a}_{k-1}). \quad (74)$$

In the previous formulation, we see that the L_2 component is not transported and does not contribute in the new momentum. Finally, the momentum only contains the contribution of the current L_2 regularization. It means that the RT transformation decouples the L_2 regularization and thus neutralizes the third effect.

We can note that R and T are commutative and that we can combine them in a simple concise scalar expression:

$$\text{RT}(\mathbf{a}_{k-1}) \stackrel{\text{def}}{=} \frac{\langle \mathbf{x}_k, \mathbf{x}_{k-1} \rangle \mathbf{a}_{k-1} - \langle \mathbf{x}_k, \mathbf{a}_{k-1} \rangle \mathbf{x}_{k-1}}{\langle \mathbf{x}_k, \mathbf{x}_k \rangle}, \quad (75)$$

$$\mathbf{a}_k = \beta \text{RT}(\mathbf{a}_{k-1}) + \nabla \mathcal{L}(\mathbf{x}_k) + \lambda \mathbf{x}_k. \quad (76)$$

This new momentum leads to $\mathbf{c}_k = \mathbf{c}_k^{\text{RT}} + r_k^2 \lambda \mathbf{u}_k$ with $\langle \mathbf{c}_k, \mathbf{u}_k \rangle = \lambda r_k^2$ and $\mathbf{c}_k^\perp = \mathbf{c}_k^{\text{RT}}$. The latter relies only on the trajectory on the hypersphere and always lies in the tangent space:

$$\mathbf{c}_k^{\text{RT}} = \beta \Gamma_{\mathbf{u}_{k-1}}^{\mathbf{u}_k}(\mathbf{c}_{k-1}^{\text{RT}}) + \nabla \mathcal{L}(\mathbf{u}_k). \quad (77)$$

Details on Adam-SRT. We recall that S avoids the deformation on the momentum. The transformation RT allows us to have a momentum lying in the tangent space of the hypersphere and leads to the previously stated direction \mathbf{c}_k^{RT} . The final Adam-SRT scheme reads:

$$\mathbf{x}_{k+1} = \mathbf{x}_k - \eta_k \frac{\mathbf{m}_k}{1 - \beta_1^{k+1}} / \sqrt{\frac{v_k}{1 - \beta_2^{k+1}}} + \epsilon, \quad (78)$$

$$\mathbf{m}_k = \beta_1 \text{RT}(\mathbf{m}_{k-1}) + (1 - \beta_1)(\nabla \mathcal{L}(\mathbf{x}_k) + \lambda \mathbf{x}_k), \quad (79)$$

$$v_k = \beta_2 \frac{r_{k-1}^2}{r_k^2} v_{k-1} + (1 - \beta_2) d^{-1} \|\nabla \mathcal{L}(\mathbf{x}_k) + \lambda \mathbf{x}_k\|^2. \quad (80)$$

We also rescale the introduced scalar v_k at each step with the factor $\frac{r_{k-1}^2}{r_k^2}$. This removes the radius from the gradient contribution of the scheduling $\nu^{\text{R}} = r_k v_k$, in contrast with ν_k from Eq. (64). The new scheduling effect reads:

$$\nu_k^{\text{R}} = d^{-1/2} \frac{1 - \beta_1^{k+1}}{1 - \beta_1} \sqrt{\frac{1 - \beta_2}{1 - \beta_2^{k+1}}} \left(\sum_{i=0}^k \beta_2^{k-i} \|\nabla \mathcal{L}(\mathbf{u}_i) + \lambda r_i \mathbf{u}_i\|^2 \right)^{1/2}.$$

E Implementation details

The implementation of Adam-SRT is illustrated in Algorithm 1. The same RT transformation applies to SGD-MRT as well. Adam-S is the version of this algorithm without the RT transformation of the momentum. From a technical point of view, all experiments were ran with Python v3.6, PyTorch v1.3, CUDA 10 on NVIDIA 1080Ti GPUs.

Algorithm 1 Adam-SRT, our proposed optimization algorithm illustrated for a filter $\mathbf{x} \in \mathbb{R}^d$ followed by BN. Steps that are different from Adam are shown in highlight. For non-convolutional layers we use standard Adam.

Require: $\beta_1, \beta_2 \in [0, 1); \lambda, \eta \in \mathbb{R}; \mathcal{L}(\mathbf{x})$

- 1: **initialize** step $k \leftarrow -1$; $\mathbf{m}_k \leftarrow 0$; $v_k \leftarrow 0$; $\mathbf{x} \in \mathbb{R}^d$
- 2: **while** *stopping criterion not met* **do**
- 3: $k \leftarrow k + 1$
- 4: $\mathbf{g} \leftarrow \nabla \mathcal{L}(\mathbf{x}_k) + \lambda \mathbf{x}_k$
- 5: $\mathbf{m}_k \leftarrow \beta_1 \mathbf{m}_{k-1} + (1 - \beta_1) \mathbf{g}$
- 6: $v_k \leftarrow \beta_2 v_{k-1} + (1 - \beta_2) d^{-1} \mathbf{g}^\top \mathbf{g}$
- 7: $\hat{\mathbf{m}} \leftarrow \mathbf{m}_k / (1 - \beta_1^{k+1})$
- 8: $\hat{v} \leftarrow v_k / (1 - \beta_2^{k+1})$
- 9: $\mathbf{x}_{k+1} \leftarrow \mathbf{x}_k - \eta \hat{\mathbf{m}} / (\sqrt{\hat{v}} + \epsilon)$
- 10: $\mathbf{m}_k \leftarrow \mathbf{m}_k (\mathbf{x}_{k+1}^\top \mathbf{x}_k \mathbf{m}_k - \mathbf{m}_k^\top \mathbf{x}_{k+1} \mathbf{x}_k) / (\mathbf{x}_{k+1}^\top \mathbf{x}_{k+1})$
- 11: $v_k \leftarrow v_k (\mathbf{x}_k^\top \mathbf{x}_k / \mathbf{x}_{k+1}^\top \mathbf{x}_{k+1})$
- 12: **return** resulting parameters \mathbf{x}_k

Table 3: Best learning rate and momentum factor. We systematically found the same learning rate for each dataset and architecture while the momentum factor was fixed to 0.9.

Method	η_0	β, β_1
SGD-MRT	0.1	0.9
Adam-S	0.001	0.9
Adam-SRT	0.001	0.9
SGD-M	0.1	0.9
Adam	0.001	0.9
AdamW	0.001	0.9
AdamG	0.01	0.9

E.1 Training and implementation details

For each optimization scheme, each dataset and each architecture, the same grid search was performed while batch size was fixed. We used a batch size of 128 for SVHN, CIFAR10, CIFAR100 and 256 for ImageNet. The learning rates η varied in $\{10^{-4}, 10^{-3}, 10^{-2}, 10^{-1}\}$, the weight decay in $10^{-3} \cdot \{0, \frac{1}{128}, \frac{1}{64}, \frac{1}{32}, \frac{1}{16}, \frac{1}{8}, \frac{1}{4}\}$ (similar to [15]), the momentum was fixed to 0.9 (β for SGD and β_1 for variants of Adam) and the order-two moment β_2 in $\{0.99, 0.999, 0.9999\}$ (as in [8]).

We used the same step-wise learning rate scheduler for each method. For SVHN, CIFAR10 and CIFAR100, models were trained during 405 epochs, and the learning rate multiplied by 0.1 at epochs 135, 225 and 315. On ImageNet, models were trained during 135 epochs and the learning rate multiplied by 0.1 at epochs 45, 75 and 105.

The optimization schemes introduced in this paper do not change the complexity in time of the algorithm. During the update of parameters in a layer, we only do a temporary copy of the parameter tensor just before the update to perform the RT transformation. This temporary copy is flushed after the RT transformation. Nothing permanent is stored in the optimizer.

Note that, for each architecture and each dataset, the same learning rate was systematically found for each method while the momentum factor was fixed at 0.9 (cf. Table 3).

Other hyperparameters, i.e., L_2 regularization and order-2 moment, are in Table 4.

Table 4: Best L_2 regularization (λ) and order-2 moment factors (β_2).

Setup			SGD-M	Adam [8]	AdamW [15]	AdamG [7]	SGD-MRT (ours)	Adam-S (ours)	Adam-SRT (ours)
CIFAR10	ResNet20	λ	0.000250	0.000500	0.000125	0.000500	0.000031	0.000500	0.000008
		β_2	X	0.99	0.99	0.99	X	0.99	0.99
	ResNet18	λ	0.000250	0.000008	0.000063	0.000500	0.000250	0.000016	0.000008
		β_2	X	0.999	0.99	0.99	X	0.99	0.99
	VGG16	λ	0.000250	0.000031	0.000250	0.000500	0.000063	0.000031	0.000016
		β_2	X	0.999	0.999	0.999	X	0.999	0.999
CIFAR100	ResNet18	λ	0.000500	0.000125	0.000125	0.000125	0.000500	0.000125	0.0
		β_2	X	0.999	0.99	0.99	X	0.99	0.999
	VGG16	λ	0.000500	0.000063	0.000016	0.000063	0.000125	0.000063	0.000008
		β_2	X	0.99	0.99	0.99	X	0.99	0.99
SVHN	ResNet18	λ	0.000500	0.0	0.000008	0.000500	0.000500	0.000031	0.000008
		β_2	X	0.999	0.999	0.99	X	0.99	0.999
	VGG16	λ	0.000500	0.0	0.000031	0.000500	0.000031	0.000008	0.000250
		β_2	X	0.99	0.99	0.99	X	0.99	0.999
ImageNet	ResNet18	λ	0.000063	0.000008	X	X	0.000063	0.000016	0.000008
		β_2	X	0.99	X	X	X	0.99	0.999

Table 5: Comparison of optimization scheme. The figures in this table are the mean top1 accuracy (and the standard deviation) over 5 seeds on the test set for CIFAR10, CIFAR100 and on the validation set for SVHN, and over 3 seeds for ImageNet. The RT transformation of the momentum was only performed on \mathcal{F} (set of filters parameters) while the remaining were trained with SGD.

Method	CIFAR10			CIFAR100		SVHN		ImageNet
	ResNet20	ResNet18	VGG16	ResNet18	VGG16	ResNet18	VGG16	ResNet18
SGD-M	92.39 (0.12)	95.10 (0.04)	93.56 (0.05)	77.08 (0.18)	73.77 (0.10)	95.96 (0.15)	95.95 (0.09)	69.86 (0.06)
SGD-MRT (ours)	92.25 (0.12)	94.93 (0.23)	93.68 (0.30)	77.09 (0.15)	73.32 (0.29)	96.17 (0.12)	95.95 (0.12)	69.76 (0.15)

E.2 Empirical study of SGD-MRT

In the case of SGD, as can be seen in Table 5, the improvement in terms of performance of the RT transformation to the momentum is less systematic. The standard deviation is often higher, which indicates less stability with SGD-MRT. The reasons why the RT transformation improves systematically Adam-S and not SGD-M remain an open question.

E.3 Implementation details of tracking

Regarding tracking experiments, to make the comparison possible between different tracked quantities, we use the following strategy: only parameters in convolutional layers followed by a BN layer are trained using hyperparameters from Table 3 and Table 4 with constant learning rate during 150 epochs. Meanwhile, BN and fully-connected-layer parameters are frozen to values reached after a previous training of a vanilla SGD-M using an initial learning rate of 0.1, a L_2 regularization factor of 0.0001 and a constant learning rate scheduler during 150 epochs.